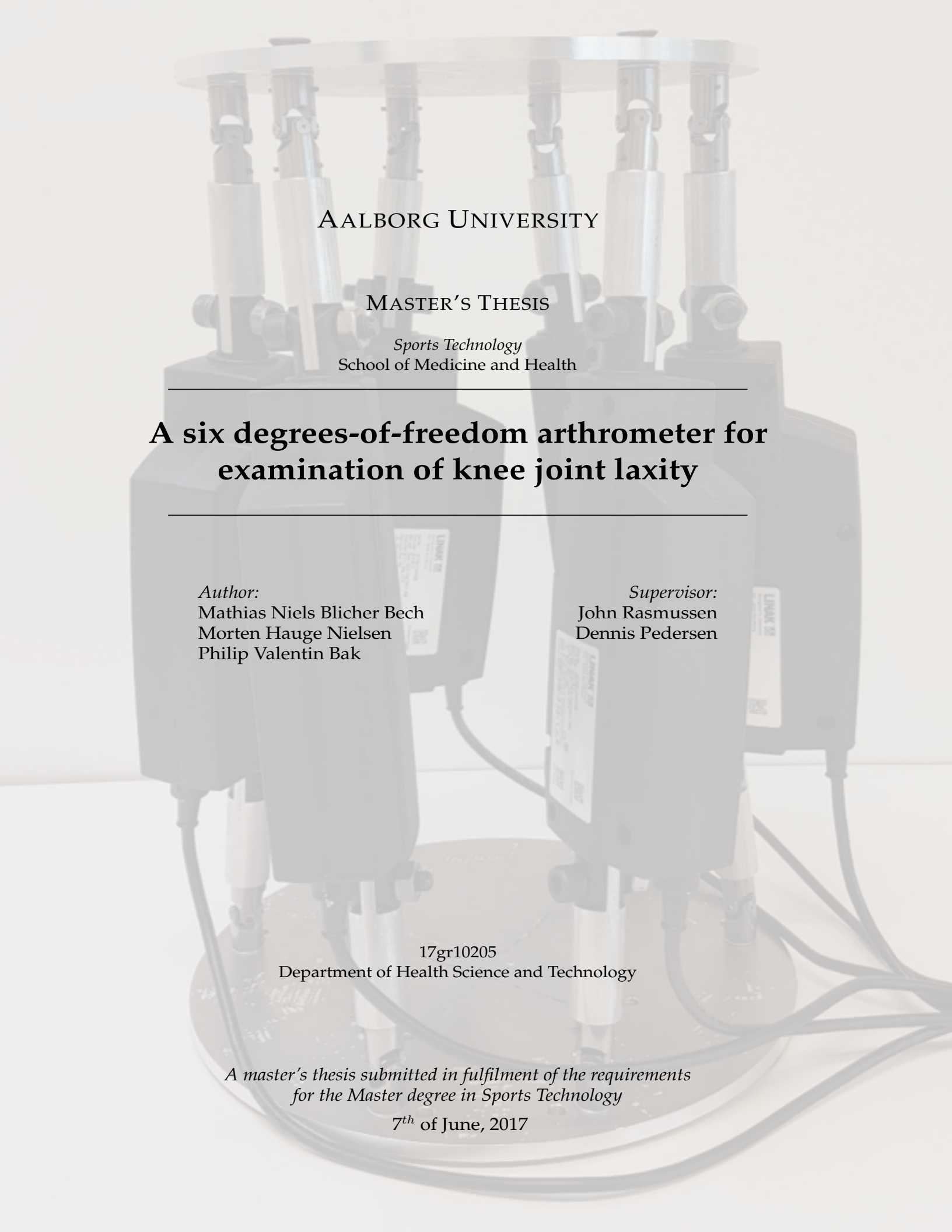

AALBORG UNIVERSITY

MASTER'S THESIS

Sports Technology
School of Medicine and Health

A six degrees-of-freedom arthrometer for examination of knee joint laxity

Author:
Mathias Niels Blicher Bech
Morten Hauge Nielsen
Philip Valentin Bak

Supervisor:
John Rasmussen
Dennis Pedersen

17gr10205
Department of Health Science and Technology

A master's thesis submitted in fulfilment of the requirements for the Master degree in Sports Technology

7^{th} of June, 2017

School of Medicine and Health

Fredrik Bajers Vej 7

9220 Aalborg Ø

http://www.smh.aau.dk/

Title: A six degrees-of-freedom arthrometer for examination of knee joint laxity

Theme: Application of Scientific Methods in Sports Technology

Sports Technology: Master's thesis - Spring 2017

Researchgroup: 17gr10205

Authors:

Mathias Niels Blicher Bech

Morten Hauge Nielsen

Philip Valentin Bak

Supervisors:

John Rasmussen

Dennis Pedersen

Number of pages: 75

Deadline: 07-06-2017

Introduction: Knee joint laxity may cause knee instability and is associated with the risk of knee injuries and subsequent condition such as osteoarthritis. The current methods of measurements have several limitations, including non-quantifiable measurements and one-dimensionality. The aim of the current thesis was to develop an arthrometer with six degrees-of-freedom to assist examination of static knee joint laxity. ***Methods:*** The arthrometer consists of a top and bottom platform linked with six linear actuators. Simulations of length and size were conducted in the AnyBody Modelling System while the durability of the top platform was assessed through a finite element analysis in SolidWorks. A motion capture test was performed to verify the range of motion (ROM) compared to the laxity values in the current literature. The ROM was tested by positioning the arthrometer in the anterior-posterior (AP), varus-valgus (VV), and internal-external (IE) end position. ***Results:*** The maximum AP translation, VV rotation and IE rotation were found to be 383.41 mm, 18.97°, and 90.17°, respectively. ***Discussion:*** The arthrometer has the potential to stress individual ligaments in the knee joint, hence assist the examination of static knee joint laxity. Furthermore, it provides the opportunity to combine movements and forces in multiple planes.

Abstract

Introduction: Knee joint laxity may cause knee instability and is associated with the risk of knee injuries. Injuries increase the probability to develop subsequent conditions such as osteoarthritis. The current methods of measurements have several limitations, including non-quantifiable measures and one-dimensionality. The aim of the current thesis was to develop an arthrometer with six degrees-of-freedom to assist examination of static knee joint laxity.

Methods: The arthrometer consists of a top and bottom platform linked with six linear actuators to provide the required mobility. Simulations of the length and size were conducted in the AnyBody Modelling System while the durability of the top platform was assessed through a finite element analysis in SolidWorks. A simplified motion capture test was performed to verify the range of motion (ROM) of the arthrometer compared to the highest laxity values found in the current literature. The ROM was tested by manually positioning the arthrometers in the end positions during three different examinations i.e. anterior-posterior (AP) translation, varus-valgus (VV) rotation, and internal-external (IE) rotation.

Results: The maximum AP translation, VV rotation and IE rotation were found to be 383.41 mm, 18.97°, and 90.17°, respectively.

Discussion: The arthrometer presented has the potential to stress individual ligaments in the knee joint, hence assist the examination of static knee joint laxity. Furthermore, it provides the opportunity to combine movements and forces in multiple planes.

Keywords: *Knee joint laxity, Arthrometry, Parallel link mechanism, Simulations, Range of Motion*

Resume

Dette kandidatspeciale er udarbejdet i perioden fra den 1. februar til den 7. juni 2017 på kandidatuddannelsen i Sports Technology ved Aalborg Universitet. Specialet omhandler udvikling af et arthrometer med seks frihedsgrader, som kan assistere klinikere i statiske undersøgelser af slaphed i knæleddet.

Forståelsen af knæleddet er vigtigt, da skader heri kan videreudvikle sig til efterfølgende kroniske tilstande, såsom slidgigt (Kakarlapudi 2001, Thomas et al. 2016). Slaphed i knæleddet kan medføre ustabile knæled og er associeret med risikoen for udviklingen af knæskader (Küpper et al. 2007, Taylor et al. 2015).

Slaphed kan defineres som tilstanden af strukturen i et led. Dette betegner mængden af bevægelse, udelukkende begrænset af ligamenter og brusk, når et led udsættes for en ekstern kraft (Küpper et al. 2007). Slaphed i knæleddet kan inddeles i tre typer: anterior-posterior (AP), varus-valgus (VV) og intern-ekstern (IE) slaphed. På nuværende tidspunkt er undersøgelserne af slaphed i knæleddet direkte påvirket af subjektivitet og erfaring, og begrænsede til kun at teste en type slaphed. Derfor vil en metode til kvantitativ og standardiserede målinger være fordelagtig.

Med afsæt i de nuværende metoders begrænsninger og problematikker ved undersøgelse af slaphed i knæleddet, fokuserer dette speciale på udviklingen af et arthrometer, som kan belaste individuelle ligamenter i henhold til de typer af slaphed. Ved at implementere principperne fra en Stewart Platform med seks frihedsgrader, kan tre translative bevægelser og tre rotatoriske bevægelser udføres af arthrometeret. Ved at anvende arthrometeret, bestående af en top- og bundplade samt seks lineære aktuatorer, i forening med en kraftmåler og en EOS røntgen scanner, kan objektive in-vivo målinger af slaphed i knæleddet foretages.

Der blev foretaget beregninger af den maksimale bevægelsesmængde og belastningsevne i hver af de tre typer af slaphed, i henhold til den nuværende litteratur. Computersimuleringer vedrørende længden og størrelsen af arthrometeret og de lineære aktuatore blev udført i AnyBody Modeling software (AnyBody Technology A/S, Aalborg, Denmark). Efterfølgende blev toppladens egenskaber testet ved brug af 'Finite Element Analysis' i SolidWorks CAD software v.2015x64 Edition SP5.0 (Dassault systems, SolidWorks Corp., Massachusetts, USA). Til at verificere arhrometerets bevægelsesmængde, blev et motion capture studie udført ved brug af Qualisys Track Manager software (Qualisys, Göteborg, Sverige).

Ud fra computersimuleringerne blev seks aktuatorer fra Linak (Linak A/S, Silkeborg, Danmark) af modellen LA12 med en længde på 245 mm og en slaglængde på 100 mm anvendt. Derudover blev en top- og bundplade radius på henholdsvis 100 og 125 mm fremstillet i en 7075-T6 aluminiums legering med tykkelsen 8 mm.

Ud fra motion capture studiet blev arthometerets maksimale bevægelsesmængde i AP translation, VV- og IE rotation bestemt til henholdsvis 383.41 mm, 18.97° og 90.17°.

Ud fra metoden præsenteret i nærværende studie, har dette arthrometer potentialet til at kunne stresse ligamenter i knæleddet og derved hjælpe ved statiske undersøgelser af tre typer af slaphed i knæleddet.

Preface

This master's thesis is written in the period from the 1st of February to the 7th of June, by three graduate students enrolled in the Sports Technology masters programme in the Department of Health Science and Technology at Aalborg University.

The master's thesis is addressed to readers with knowledge of human anatomy, biomechanics, computational modelling and product development.

References are presented according to the Harvard method: If the reference is placed after punctuation in a section, the reference refers to the whole section, whereas if placed before punctuation, it relates to the sentence.

Figures, Tables, and equations are named continuously in relation to the number of the chapter, e.g. Figure 3.1 refers to the first figure in the third chapter. Furthermore, additional elaborations can be found in the appurtenant appendix.

Acknowledgement

The authors would like to acknowledge John Rasmussen and Dennis Pedersen for their supervision and guidance. Furthermore, thanks to Linak A/S, Silkeborg, Denmark for providing linear actuators, cables and power supplies. The present thesis was funded by the Danish Council for Independent Research under Grant No. DFF-4184-00018.

Contents

1 Introduction **1**

2 Description of arthrometer **4**

3 Theoretical background **6**

3.1 Knee anatomy . . . 6

3.1.1 The knee joint . . . 6

3.1.2 Knee instability . . . 7

3.1.2.1 Knee laxity . . . 8

3.1.2.2 Limitations . . . 10

3.1.2.3 Stress radiography . . . 10

3.2 Computational modelling . . . 11

3.2.1 AnyBody Modeling System . . . 11

3.2.1.1 Kinematic analysis . . . 12

3.2.1.2 Inverse dynamic analysis . . . 12

3.2.1.3 Parameter study . . . 13

3.2.2 Finite element analysis . . . 13

3.2.2.1 Finite element method . . . 14

3.2.2.2 SolidWorks . . . 15

3.3 Mechanical manipulators . . . 15

3.3.1 Stewart platform . . . 16

3.3.1.1 Position of joints . . . 16

3.3.1.2 Linear actuators . . . 18

3.3.1.3 Kinematics and dynamics of a Stewart platform . . . 19

3.4 EOS X-ray scanner . . . 21

3.4.1 Principles of the EOS X-ray scanner . . . 21

3.4.2 Practical implications . . . 23

3.4.3 3D knee laxity measurements . . . 23

4 Concept development **25**

4.1 Product requirements . . . 25

4.1.1 Current problems . . . 25
4.1.2 User needs . . . 26
4.1.3 Specific product requirements . . . 26
4.2 Conceptual idea . . . 27
4.2.1 Final design . . . 28

5 Arthrometer development **30**
5.1 Calculations of range of motion and load capacity . . . 30
5.1.1 Anterior-posterior laxity . . . 30
5.1.2 Varus-valgus laxity . . . 31
5.1.3 Internal-external laxity . . . 31
5.2 Arthrometer size . . . 31
5.2.1 Considerations regarding dimensions and ROM . . . 33
5.2.2 Size limitations for arthrometer . . . 34
5.3 AnyBody simulations . . . 34
5.3.1 First model iteration . . . 35
5.3.2 Second model iteration . . . 35
5.4 Parameter study . . . 36
5.4.1 Boundary conditions . . . 36
5.4.2 Laxity tests . . . 37
5.4.2.1 Anterior-posterior . . . 37
5.4.2.2 Varus-valgus . . . 38
5.4.2.3 Internal-external . . . 38
5.4.2.4 Output of interest . . . 38
5.5 Selection process . . . 39
5.5.1 Results and analyses . . . 39
5.5.2 Final configuration . . . 40

6 Platform properties **43**
6.1 Finite element analysis . . . 43
6.1.1 Boundary conditions . . . 44
6.1.1.1 Mesh . . . 44
6.2 Results . . . 45
6.2.1 Final configuration . . . 46

7 Verification of range of motion **47**

7.1 Test setup . . . 47

7.2 Test protocol . . . 48

7.2.1 Anterior-Posterior range of motion . . . 48

7.2.2 Varus-valgus range of motion . . . 49

7.2.3 Internal-external range of motion . . . 50

7.3 Data processing . . . 51

7.3.1 Anterior-posterior . . . 51

7.3.2 Varus-valgus . . . 51

7.3.3 Internal-External . . . 52

7.3.4 Displacement of the top platform . . . 52

7.4 Results . . . 53

8 Discussion **54**

8.1 Verification of range of motion . . . 54

8.1.1 Anterior-posterior . . . 54

8.1.2 Varus-valgus . . . 55

8.1.3 Internal-external . . . 55

8.2 Arthrometer development . . . 55

8.3 Finite element analysis . . . 56

9 Conclusion **58**

Bibliography **59**

A Appendix **65**

A.1 Technical Drawings . . . 65

A.1.1 LA12 . . . 65

A.1.2 Top Platform . . . 66

A.1.3 Bottom platform . . . 67

A.1.4 Linking part . . . 68

A.1.5 RS Pro universal joint . . . 69

A.2 Components . . . 70

A.3 AnyBody simulations . . . 71

Introduction 1

The understanding of knee instability has been given a lot of attention during the last decade, as the knee joint is key for successful locomotion during physical activity (Küpper et al. 2007). Additionally, injuries concerning the knee joint increase the likelihood of subsequent conditions, such as the development of osteoarthritis (Kakarlapudi 2001, Thomas et al. 2016). Knee instability may have implications for long-term injuries or degeneration and has been associated with greater risk of knee injury, knee joint pain, functional loss, and health care expenditures due to out-of-plane motions and high-risk movement strategies during weight bearing activities (Küpper et al. 2007, Taylor et al. 2015). Thus, improved understanding of knee instability is advantageous.

In the current literature regarding knee instability, several gaps exist. These possess a challenge for clinicians during evaluation, treatment, and rehabilitation, due to the complexity of the knee joint. During dynamic activities, it exhibits six degrees-of-freedom (DOF), which can be identified as three rotations (flexion-extension, external-internal, and varus-valgus) and three translations (anteroposterior, medial-lateral, and superior-inferior) (Komdeur et al. 2002). During dynamic activities, knee joint instability is clinically described as symptoms of buckling, shifting, giving way or involuntary movements of the knee joint (Schmitt et al. 2008). When diagnosing knee instability, clinicians rely on patients reporting these symptoms (Schmitt et al. 2008).

The stability of the knee joint is primarily maintained by seven ligaments and secondarily by the muscle groups acting at the joint (Martini et al. 2012). Therefore, the most common reason for knee instability is ligament injury, where non-contact activities involving jumping, twisting, cutting and sudden deceleration are the most frequent movements causing knee instability (Shultz et al. 2012). Furthermore, excessive knee joint laxity may cause instability. The terms knee instability and knee joint laxity are often used interchangeably, although they are not defined identically (Schmitt et al. 2008). Laxity is defined as the condition of the joint structure and is a quantification of joint movements within the constraints of ligaments and cartilage without any muscular activity when the joint is affected by an external force (Küpper et al. 2007).

Several researchers have previously investigated the extent of knee joint laxity in different applications

(Musahl et al. 2017). A frequent way to compartmentalise knee joint laxity is by classifying it into three categories: Anterior-posterior (AP), varus-valgus (VV), and internal-external (IE) laxity. AP laxity is a uni-planar displacement in the sagittal plane while VV and IE laxity are angular displacements in the frontal and transverse plane, respectively (Bignozzi et al. 2010, Shultz et al. 2012). Quantification of knee joint laxity is essential, due to joint instability related pain and injuries (Moewis et al. 2014, Musahl et al. 2017).

Knee joint laxity can be assessed both statically and dynamically. Static examinations of laxity imply uni-planar examinations of the knee, e.g. the Lachman test or the Anterior drawer test, while dynamic examinations imply examination in multiple planes e.g. by employing the Pivot Shift Test, which is often considered to be the gold standard for evaluation of rotatory knee joint laxity (Van Eck et al. 2013, Sundemo et al. 2016). During both static and dynamic examination, the ligaments are stressed individually to assess the magnitude of the specific knee joint laxity (Kakarlapudi 2001).

In contrast to the static examination, the pivot shift test is a complex procedure, characterised by identifying a subject specific combination of valgus moment and iliotibial force necessary to allow the pivot shift to occur (Markolf et al. 2008). Hence, these examinations can be difficult to assess accurately, as the results rely on the examiner's experience, due to the lack of a standard examination procedure. (Scholten et al. 2003, Mouton et al. 2012)

Researchers have been trying to mechanise and standardise both static and dynamic examinations of knee joint laxity since a device which could apply specific forces and moments would improve the examination of knee joint laxity (Musahl et al. 2017). However, the complex movement during a dynamic examination has entailed increased attention on devices examining knee joint laxity statically rather than dynamically (Mouton et al. 2012). The objectivity of a static AP laxity examination can be improved using the KT-1000 or KT-2000 arthrometer, which quantifies the AP-translation objectively by applying a force to the tibia (Adler et al. 1995, Ganko et al. 2000, Shultz et al. 2012, Miyazaki et al. 2012, Mouton et al. 2012, Van Eck et al. 2013).

Additionally, when performing a static examination of VV and IE laxity, various custom built devices are often used, due to the lack of a commercial clinical device (Shultz et al. 2007). Even though the current arthrometers available provide objective quantification of knee joint laxity, the methods are limited to examining one type of laxity (AP, VV, and IE), hence examination in one plane. Other limitations to the current arthrometry include that the results are affected by the experience of the examiner due to the lack of standardisation of the direction and rate of the applied force. In addition, patient collaboration is necessary to obtain reliable measurements, since muscular activity can bias the amount of laxity. Furthermore, any influence from soft-tissue artefacts can affect the amount of laxity (Musahl 2017). Therefore, an arthrometer,

allowing objective quantification and examination of all types of laxity would be beneficial.

Zantop et al. (2007) examined knee kinematics using a six-joint serially articulated robotic manipulator, which allows movement in DOF. The manipulator was used to move the joint into the desired position during an examination of knee kinematics. Thereby, the six DOF manipulator provided the ability to examine all types of laxity as opposed to the current clinically available arthrometers, thus, resolving the limitation regarding the one-dimensionality. However, the serial manipulator entails a low load capacity due to the cantilever structure. Additionally, the positioning capability is weak if the manipulator is to move in a large workspace. As opposed to the serial manipulator, the parallel manipulator offers a high load capacity and a precise positioning capability. (Dasgupta & Mruthyunjaya 2000, Küçük 2012)

An alternative to arthrometers for examination of knee joint laxity is stress radiography. This method has been proven to be more accurate than arthrometers regarding laxity quantification (Garavaglia et al. 2007). Despite the higher accuracy, this method is limited with regards to one-dimensionality, non-quantifiable results, and radiation exposure (Balonov & Shrimpton 2012). The EOS X-ray scanner significantly reduces the affection of radiation exposure and provides the opportunity to capture X-ray images in two dimensions (Illés & Somoskeöy 2012). Pedersen et al. (2017) proposed a method where the EOS X-ray scanner is implemented to allow objective quantification of static knee joint laxity.

Based on the limitations regarding the current methods for examination of knee joint laxity, the aim of the present thesis was to develop an arthrometer, based on the principles of a six DOF parallel manipulator, to assist objective examination of static knee joint laxity by stressing the ligaments according to the AP, VV and IE laxity examinations. The arthrometer should afterwards be used in conjunction with an EOS X-ray scanner to obtain objective examinations of AP, VV, and IE laxity.

Description of arthrometer 2

The arthrometer presented in the present thesis is designed to resolve the limitations of the current methods for examination of static knee joint laxity. It is based on the principles of a parallel manipulator, which have six DOF, thereby providing the required DOF to enable examination of VV, AP and IE laxity. The arthrometer consists of a top and bottom platform, six linear actuators, 12 custom built linking parts, and additional bolts and nuts (Figure 2.1).

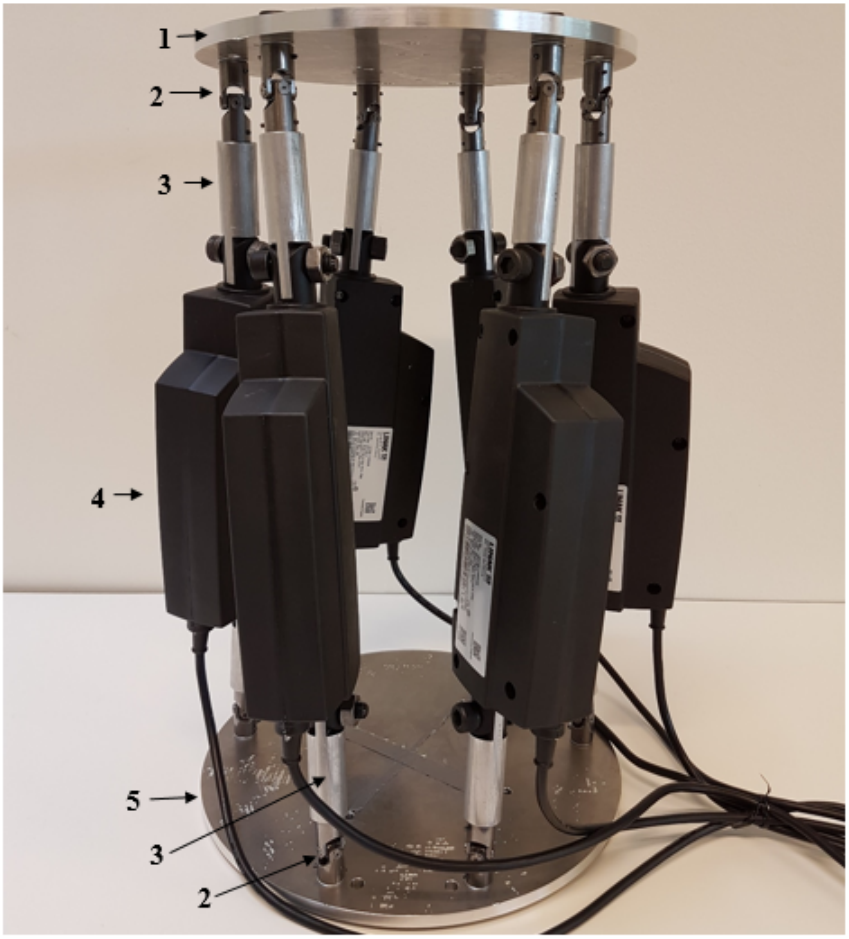

Figure 2.1: The arthrometer including the top platform (1), universal joints (2), linking parts (3), linear actutators (4), and the bottom platform (5).

The top and bottom platforms are constructed with a thickness of 8 mm in 7075-T6 aluminium alloy, which has a yield strength of 505 MPa and a density of 2810 Kg/m^3. Six symmetrically distributed holes were

drilled in each platform for attachment of the linear actuators. The holes are located in three joint-pairs separated by 120°, and the holes in a joint pair are separated by 40° (Appendix A.1.2 and A.1.3). Additional symmetrically distributed holes were drilled in the top platform for attachment of the force sensor with 20° separating these joint pairs.

The six linear actuators was the LA12 model from Linak (Linak A/S, Silkeborg, Denmark) with a minimum built-in-dimensions (BID) of 245 mm and a stroke length of 100 mm, connects the top and bottom platform (Appendix A.1.1). In addition, they can produce a maximum force of 750 N and a maximum velocity of 40 mm/sec. The LA12 actuators have integrated potentiometers with 0-10 V feedback for position control. The actuators provide the required mobility by a combination of extension and shortening of the actuators.

Linking parts connects the actuators to the joints on the platforms and extends the actuators to comply with the required lengths needed to examine static knee joint laxity. The linking parts have a length of 88 mm, where 27 mm in one of the ends are used for the attachment of the actuator, and 11 mm at the other end are used for attachment of the joint (Appendix A.1.4). Thus, the linking parts extend each actuator with 122 mm.

Twelve RS pro universal joints (RS components, Copenhagen, Denmark), with a length of 40 mm, a hub diameter of 16 mm, and a hole diameter of 8 mm, connect the linking parts to the top and bottom platform (Appendix A.1.5). The universal joints were mounted on the platforms with bolts, fixated with a pin. The bolts can rotate in the hole, hence, the universal joints with the additional rotation function as spherical joints.

Additional bolts and nuts were used for the final assembly of the arthrometer. This involves 12 M10x35 mm bolts, 12 M8x25 mm bolts, 12 nuts (Ø10 mm), 12 washers, and 24 pins (Appendix A.2).

Theoretical background 3

The aim of this chapter is to provide a progressive elaboration of the underlying theoretical background for development of a arthrometer for examination of knee joint laxity. The content includes theoretical sections regarding knee anatomy, computational modelling, mechanical manipulators, and EOS X-ray scanner.

3.1 Knee anatomy

In the following section the basic anatomy of the knee will be described, including the knee joint, knee instability, and the DOF of the knee.

3.1.1 The knee joint

The complexity of the knee joint renders it to act as a hinge joint, allowing weight transfer from the femur to the tibia. It is a bicondylar joint, consisting of three separate articulations: one between the patella and the patellar surface of the femur and two between the medial and lateral condyles of femur and tibia, respectively. These articulations permit movement in six DOF, three rotational (flexion-extension, external-internal, and varus-valgus) and three translational (anteroposterior, medial-lateral, and compression-distraction). Seven major ligaments-tendons act to stabilise the joint (Figure 3.1), and therefore, complete dislocations are very rare. (Komdeur et al. 2002, Martini et al. 2012) The seven major ligaments/tendons are:

- A tendon, which originates primarily at the quadriceps femoris and crosses the anterior surface of the knee joint, encasing the patella, where it is attached to the anterior surface of the tibia. This tendon includes the quadriceps tendon, patellar retinaculum, and the patellar ligament.
- Two popliteal ligaments, which are attached to the femur and the heads of the tibia and fibula on the posterior surface of the knee joint.
- The anterior cruciate ligament and posterior cruciate ligament are located in the joint capsule attached to the intercondylar area of the tibia and the condyles of the femur. The ACL and PCL are crossing

ligaments limiting anterior and posterior displacement of the tibia while maintaining the structure of the femoral and tibial condyles.

- The medial collateral ligament and lateral collateral ligament reinforce the medial and lateral surfaces of the knee joint, respectively, thus, limiting displacement in the frontal and transverse plane.

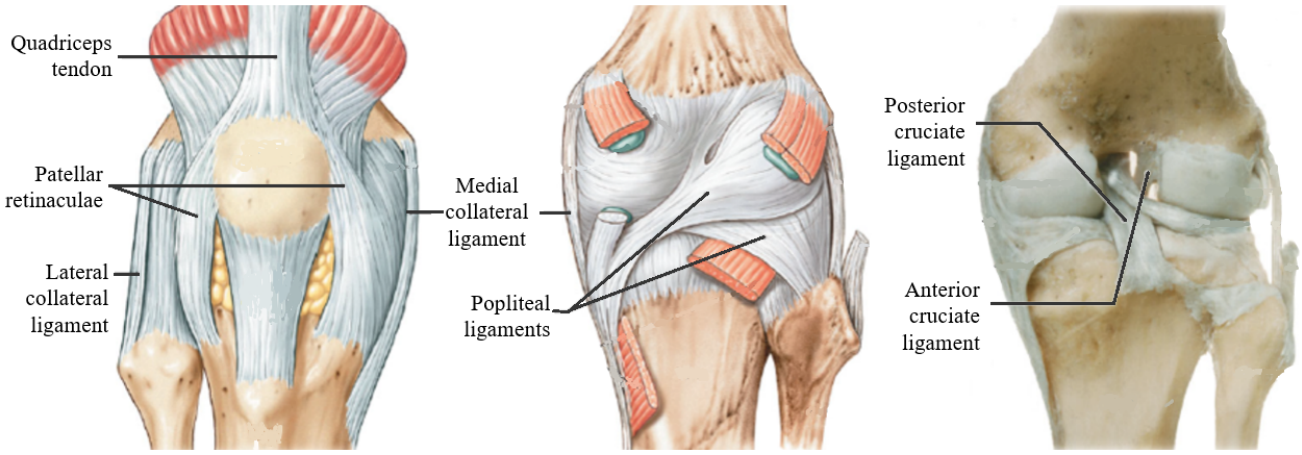

Figure 3.1: Anterior view of the superficial layer (left), posterior view of the superficial layer (centre), and deep posterior view (right) of the knee joint including the seven major ligaments-tendons (Modified from Martini et al. (2012)).

When the knee joint is extended, the tibia makes a small rotation which clamps the lateral meniscus between the tibia and femur, due to the ACL being tightened. Thus, when the knee joint is fully extended, it is locked in an extended position. This locked position makes humans able to stand for longer periods without actively using the extensor muscles. A muscular contraction is needed to unlock the joint, as this rotates the tibia medially and the femur laterally. (Martini et al. 2012)

3.1.2 Knee instability

The understanding of knee instability has been given much attention during the last decade, as the knee joint is key for successful locomotion. Despite this, several gaps in the current knowledge still possess a challenge for clinicians during evaluation, treatment, and rehabilitation, due to the complexity of the knee joint. (Kakarlapudi 2001)

The stability of the knee joint is primarily maintained by seven major ligaments and secondarily by the muscle groups acting at the joint. Therefore, the most common reason for knee instability is ligament injury, where non-contact activities involving jumping, twisting, cutting, and sudden deceleration are the most frequent movements to cause knee instability. To assess the extent of a ligament injury, examinations must include plain radiography of the knee to determine any fractures, avulsions, osteochondral fragments,

or the fluid level of a hemarthrosis. Furthermore, several static and dynamic examinations of laxity can be performed such as the Lachman test and the Pivot-Shift Test. (Kakarlapudi 2001)

3.1.2.1 Knee laxity

Several researchers have investigated the extent of knee laxity in different applications (Adler et al. 1995, Sharma et al. 1999, Ganko et al. 2000, Martelli et al. 2007, Colombet et al. 2007, Song et al. 2009, Yamamoto et al. 2010, Hoshino et al. 2012, Miyazaki et al. 2012, Shultz et al. 2012, Freisinger et al. 2016, Jean-Yves et al. 2017). The most frequent way to describe knee laxity is by dividing it into three different types: AP, VV, and IE. For examination of these, two main methods are available; static and dynamic examination (Bignozzi et al. 2010). Static examinations are assessed through uniplanar movements of the joint, while dynamic examinations are assessed in multiple planes (Sundemo et al. 2016, Van Eck et al. 2013). During static and dynamic examination the ligaments are stressed individually to determine the magnitude of the injury (Kakarlapudi 2001).

Anterior-posterior laxity

The Lachman test, the Anterior drawer test, and the KT-1000/2000 arthrometers are often used to examine AP laxity. The Lachman test and the Anterior drawer test are both physical examinations manually performed by an examiner. The KT-1000/2000 is a machine that quantifies the AP-translation mechanically by applying a force anterior to the tibia while measuring the displacement of the tibia relative to the femur (Adler et al. 1995, Ganko et al. 2000, Shultz et al. 2012, Miyazaki et al. 2012). Values from different AP laxity tests in the current scientific literature can be seen in Table 3.1.

Table 3.1: Anterior-posterior knee joint laxity values reported in the current literature, and how they are examined.

Article	**Method**	**Force** [N]	**Knee flexion angle** [deg]	**Displacement** [mm]
Ganko et al., (2000)	Roliometer	67	25	10.6 ± 3.0
Ganko et al., (2000)	KT-1000	89	25	11.4 ± 2.9
Shultz et al., (2012)	KT-2000	130	25±5	8.5 ± 2.0
Miyazaki et al., (2012)	KT-2000	134	20	7.5 ± 2.0
Yves et al., (2017)	GNRB	250	20	9.2 ± 2.8
Yamamoto et al., (2010)	Lachman test	Manual	30 and 90	14.5 ± 3.3
Adler et al., (1995)	Lachman test	Manual	25	8.1 ± 2.6
Martelli et al., (2007)	Lachman test	Manual	30 and 90	10.9 ± 3.6
Adler et al., (1995)	Drop leg Lachman test	Manual	25	10.4 ± 3.2
Yamamoto et al., (2010)	Anterior drawer test	Manual	30 and 90	9.1 ± 2.3
Martelli et al., (2007)	Anterior drawer test	Manual	30 and 90	7.2 ± 3..9

Table 3.1 shows that researchers utilise various methods for examining AP laxity. Ganko et al. (2000) found no difference between AP laxity measured by experienced clinicians compared to the KT-1000/2000. Thus, for inexperienced examiners, it would be feasible to use an arthrometer to examine AP laxity statically.

Varus-valgus laxity

VV laxity is most commonly examined through manual physical examinations, which are useful when diagnosing the presence of injuries (Sharma et al. 1999). Despite this, the inter-examiner subjectivity entails a poor reliability, which depends mainly on the experience of the clinician. As a consequence, a standardised way of measuring VV laxity is needed (Snyder-Mackler et al. 1997, Freisinger et al. 2016). Values from different VV laxity tests in the current scientific literature are listed in Table 3.2.

Table 3.2: Varus-valgus knee joint laxity values reported in the current literature, and how they are examined.

Article	**Method**	**Torque** [Nm]	**Knee flexion angle** [deg]	**Displacement** [deg]
Shultz et al., (2012)	Motion Capture	10	20	11.3 ± 2.9
Freisinger et al., (2016)	Custom-made apparatus	10	60	5.0 ± 2.6
Sharma et al., (1999)	Custom-made apparatus	12	20	4.9 ± 0.35
Creaby et al., (2010)	Dynamometer	12	20	20.1 ± 6.4
Miyazaki et al., (2012)	Custom-made apparatus	22	20	6.98 ± 1.77
Delport et al., (2013)	Extensometer + Motion Capture	25	0, 45, and 90	6.0 ± 6.35
Martelli et al., (2007)	Custom-made apparatus	Not described	30	5.7 ± 1.8

Table 3.2 shows that custom built devices are used to examine VV laxity, indicating, that several researchers have tried to create a device for objective quantification of laxity, due to the lack of a commercial clinical device (Shultz et al. 2007).

Internal-external laxity

One of the most frequently used procedures for measuring IE laxity is the Pivot Shift Test (Musahl et al. 2017). Although this test is valuable in assessing rotation in the knee joint, it lacks standardisation in execution. Therefore, researchers have statically measured IE laxity by applying a torque around the long axis of the tibia, causing the knee joint to rotate internally and externally (Schmitz et al. 2008, Shultz et al. 2012). Values from IE laxity tests in the current scientific literature can be seen in Table 3.3.

Table 3.3: Internal-external knee joint laxity values reported in the current literature, and how they are examined.

Article	**Method**	**Torque** [Nm]	**Knee flexion angle** [deg]	**Displacement** [deg]
Shultz et al., (2012)	Motion Capture	5	20	27.8 ± 7.6
Yamamoto et al., (2010)	Pivot Shift test	Manual	NaN	25.5 ± 6.8
Colombet et al., (2006)	Pivot Shift test	Manual	NaN	27.0 ± 2.0
Martelli et al., (2007)	Custom-made apparatus	Not described	30 and 90	26.0 ± 4.5

Similar to the examination of VV laxity (Table 3.2), Table 3.3 indicates that several methods have been utilised for examination of IE laxity due to the lack of a commercially available device.

3.1.2.2 Limitations

The existing methods for static examination of knee joint laxity induce several limitations. Even though the existing arthrometers provide reliable and valid examination, they are limited to measuring laxity in one DOF. Hence, several examination methods should be performed to examine static knee joint laxity. Other limitations of the current methods involve low reliability due to inter-examiner variability, non-quantifiability during the physical examination, and soft-tissue artefacts in the custom built apparatuses.

The KT-1000/2000 has some limitations which need to be taken into account before use. Even though the inter-examiner reliability can be as high as 95 %, the reliability depends heavily on the experience of the examiner. The rate and direction of which the force is applied are uncontrolled. Thus, operational experience of the KT-1000/2000 arthrometers can be as important as during physical examinations. (Musahl et al. 2017) In addition, the examination can be affected by any muscular activity. Thus, patient collaboration is essential.

3.1.2.3 Stress radiography

Another way of assessing knee joint laxity is by use of stress radiography. Structures are positioned intentionally to induce plane stress during radiography (Shultz et al. 2005). This method is most commonly applied in the assessment of spinal disorders but is also applicable for examinations of static knee joint laxity. Stress radiography has previously been proved to be superior to arthrometers and clinical examinations, concerning tibia displacement quantification. However, like the limitations for the arthrometers and clinical examinations, stress radiography is limited through one-dimensionality and quantifiability (Garavaglia et al. 2007). Another issue with the method is the possible exposure to excessive radiation for both the operator and the patient (Balonov & Shrimpton 2012).

3.2 Computational modelling

3.2.1 AnyBody Modeling System

The AnyBody Modelling System (AMS)(AnyBody Technology A/S, Aalborg, Denmark) is a text-based musculoskeletal modelling software developed at Aalborg University in 2002. Even though the AMS is primarily used for musculoskeletal modelling, it provides the opportunity to solve a wide range of modelling problems. This includes the opportunity to create a model of simple mechanical systems. (Damsgaard et al. 2006) The software was primarily designed to meet four goals:

1. Allow users to create and modify musculoskeletal models to suit different purposes.
2. Facilitate model exchange and cooperations on model development allowing thorough model examination.
3. Be numerically efficient, allowing ergonomic design optimisations on private computers.
4. Be capable of conducting body models at a practical level of complexity.

A unique modelling language named AnyScript has been developed. The AnyScript uses a declarative object-oriented language for development of dynamic models (Damsgaard et al. 2006), and consists of two sections:

1. A section where users can create and define a model in a mechanical system with interacting objects around it called the 'model section'.
2. A section containing operations and analyses available under model application called the 'study section'.

The declarative nature of the software means that AnyScript has many predefined classes and operations from which users can create objects but also perform multiple analyses, i.e., parameter tests for design requirements or optimisation tests to find the best solution. The software provides various tests to be executed such as kinematical analysis, inverse dynamic analysis, and systematic parameter variations. (Damsgaard et al. 2006)

3.2.1.1 Kinematic analysis

A kinematic analysis is a study of segments in motion without explaining the causes of the motion. In other words, the purpose of a kinematic analysis is to find the position of bodies during locomotion (Robertson & Hamill 2004). However, for the AMS to perform a kinematic analysis the model needs to be kinematically determined, i.e. have an equal amount of DOF and constraints. If there are more constraints than DOF, the system is kinematically overdetermined and if the system has more DOF than constraints the system is called kinematically indeterminate. Both scenarios would usually prevent a kinematic analysis from being conducted. (AnyBody-Technology 2017*b*)

3.2.1.2 Inverse dynamic analysis

Inverse dynamics is a branch of mechanics which involves estimation of internal forces by combining kinematics and kinetics. The analysis indirectly determines unknown forces and moments from the boundary conditions using Newton's second law (Robertson & Hamill 2004):

"In an inertial reference frame, the sum of the forces F on an object is equal to the mass m of that object multiplied by the acceleration a of the object: F=ma" (Robertson & Hamill 2004)

This means that a resultant force is split into known and unknown forces. The combined forces in the x, y and z directions are then solved through equilibrium equations. A similar process is conducted for the moments around the x, y, and z directions. (Robertson & Hamill 2004)

The AMS computes the inverse dynamics of musculoskeletal models by resolving the fundamental indeterminacy of the infinite number of equilibrium equations caused by muscle redundancy. These computations determine a fixed amount of equilibrium equations, based on theoretical criteria, thus, enabling the AMS to solve the equilibrium equations. This method is more computationally efficient compared to forwards dynamic analysis. (Damsgaard et al. 2006, Andersen et al. 2009)

However, if the model is not musculoskeletal and thereby not affected by the fundamental indeterminacy, the AMS offers a more simple solution. The class called 'AnyMechStudy' solves the inverse dynamic problem of a mechanical system through dynamic equilibrium equations. (AnyBody-Technology 2017*a*)

3.2.1.3 Parameter study

A predefined analysis in the study section is the 'ParameterStudy'. This analysis offers a systematic way of automatically run multiple analyses for several combinations of model parameters. To reduce the number of combinations in the analysis, several parameters need to be predefined as either dependent or independent variable, called design measurements and design variables, respectively. The design variables control certain parameters of an object and must always be a single number within a maximum and minimum limit. To create a design variable the user must define it as an 'AnyDesVar'. The dependent variables in a 'ParameterStudy' are the results of the analyses performed with pre-defined design variables. Before conducting the analysis, the outputs of interest must be defined as 'AnyDesMes', which is the defining class for a dependent variable. For each combination of the independent variables, one or multiple results will be saved. (AnyBody-Technology 2017*c*)

3.2.2 Finite element analysis

A good mechanical design seeks to minimise the material and cost, while keeping the optimum size, shape, etc., under consideration to maintain its functionality. Furthermore, the failure criteria should always be taken into account, as this can render a component to be useless, thus losing functionality. The physical behaviour of a component can be calculated and determined by a set of partial differential equations, derived from equilibrium equations i.e. estimation of stress and deformations of a component at critical points or for a specified load and boundary condition. (Narasaiah 2008)

By solving the equilibrium equations, thereby describing the physical behaviour, designers can regard relatively simple structures, such as beams, but when analysing complex designs, the method becomes difficult. The Finite Element Analysis (FEA) is a tool created to help design evaluation by estimating solutions for the partial differential equations for complex structures. By use of the FEA, both linear and non-linear analyses can be conducted, for calculation of von Mises stresses and displacements of a particular structure. By this method, the stress distribution and deflection of a structure in a particular loading operation (force, pressure, temperature, boundary conditions) can be estimated in a relatively precise manner. (Dassault-Systemés 2017)

3.2.2.1 Finite element method

An important thing to keep in mind is that FEA derives an estimation of the physical behaviour of a component. Prior to the FEA, a geometrical model is divided into a known amount of small, simple structures/geometries (finite elements) connected at nodes. By doing this, it becomes possible to compute the equations and describe the physical behaviour of every single element. This discretization is called Finite element modelling (FEM). (Dassault-Systemés 2017)

The discretization creates a mesh of finite elements connected by nodes. The quality of this mesh can be controlled in several different ways, which in terms gives different estimations. The quality of the mesh determines the number of finite elements; a finer mesh entails a better estimation of physical behaviour. The biggest problem when meshing is, that the computational time increases with the number of elements, simultaneously. Therefore, a way to solve this is, to make a coarse mesh with local refinement in critical areas of a geometrical model (Figure 3.2). Depending on the analysis and geometry of the structure, the mesh can be altered for best fit (tetrahedral, triangular, beam, and truss elements) either in combination or consisting of a single element type. Considerations regarding meshing could minimise the error of the estimation, leading to a more accurate FEA. However, the model used in FEA is idealised with no imperfections, whereas, in reality, there will always be imperfections and geometric tolerances. (Narasaiah 2008, Dassault-Systemés 2017).

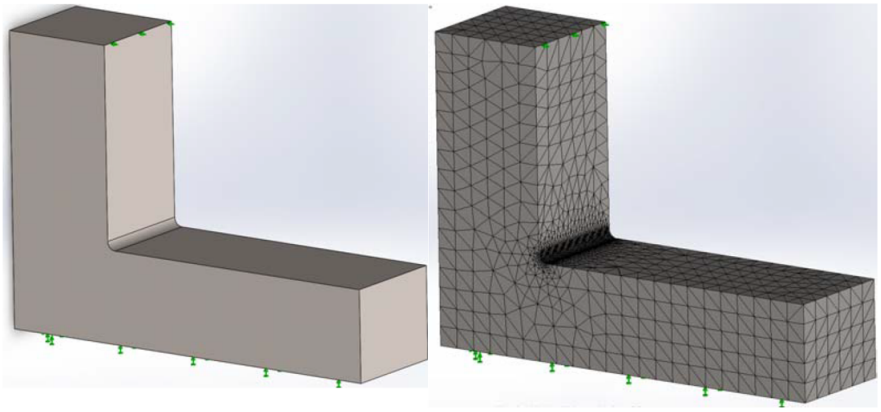

Figure 3.2: A geometry without mesh (left) and with mesh and local refinement (right).

Factor of safety

The Factor of safety (FOS) allow assessment of designs based on failure criteria. The FOS is both a way to ensure that the design does not fail but can also be used for design considerations, as a large FOS in a region indicates that materials can be saved. Depending on the application, a FOS is determined to avoid failure. (Narasaiah 2008, Dassault-Systemés 2017)

3.2.2.2 SolidWorks

SolidWorks v.2015x64 Edition SP5.0 (Dassault systems, SolidWorks Corp., Massachusetts, USA) is an easy-to-learn mechanical design automation software, which makes it possible for mechanical designers to sketch ideas quickly, experiment with features and dimensions, and produce models and detailed drawings. Furthermore, it is possible to create and conduct FEA, along with several other analyses in SolidWorks software. Besides being a great tool for mechanical designers, it permits different file extensions to be imported i.e. 3D models made from scans or CAD models created elsewhere. (Dassault-Systemés 2017)

3.3 Mechanical manipulators

The technology of robotic manipulators was originally developed to create mechanical systems with the potential of carrying out tasks normally ascribed to humans. As a consequence, the main focus was towards the open-loop serial manipulators which have the manoeuvrability similar to the human arm (Figure 3.3). However, the structure comes with a drawback as the load capacity is limited due to the cantilever structure. Furthermore, if the manipulator needs to manoeuvre in a large workspace, the positioning capability is weak. Consequently, alternative manipulators need to be used if high load capacity and precise positioning are required. Considerations of the biological world and how humans and animals utilise multiple segments to overcome high load obstacles have led to the creation of parallel manipulators. Parallel manipulators are connected to the ground with several chains attached to the end effector. This structure offers a high load capacity and has positioning capability. However, compared to serial manipulators, the workspace area is limited due to the parallel-link structure. Parallel manipulators can fundamentally be classified into two categories called planar and spatial manipulators. Planar manipulators have three DOF, which are translation along the x and y-axis and rotation around the z-axis. Spatial parallel manipulators offer six DOF, three translational and three rotational. One of the most popular parallel manipulators is the Stewart platform, which is a spatial parallel manipulator. (Dasgupta & Mruthyunjaya 2000, Küçük 2012)

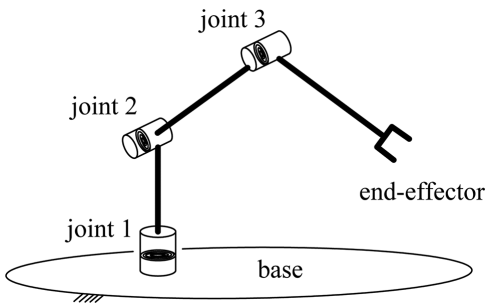

Figure 3.3: A serial manipulator with three joints connecting a base to an end-effector.

3.3.1 Stewart platform

The structure known as the Stewart platform has its origin in the design of a six DOF mechanism for simulating flight conditions (Stewart 1965). The original platform consisted of three legs connected to a platform by spherical joints. Several modifications to the original structure have resulted in the Stewart platform, as it is known today. This structure consists of two rigid structures i.e. a bottom platform and a top platform, connected by six actuators, each with spherical joints at both ends or with a spherical joint at the top platform and a universal joint at the bottom platform (Figure 3.4). This structure enables the Stewart platform to have six DOF, which indicates that the top platform can move translative in three directions and rotate around three axes either singly or in combination. These movements are performed by a combination of elongation and shortening of six linear actuators. (Dasgupta & Mruthyunjaya 2000)

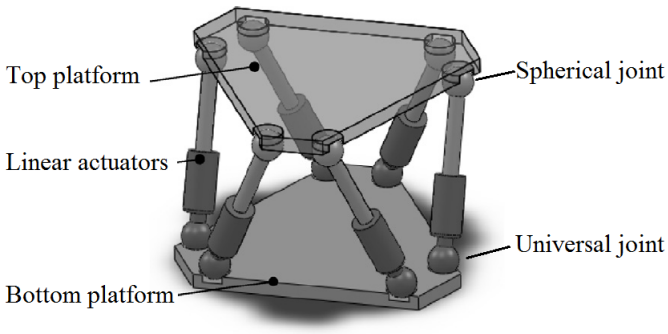

Figure 3.4: A Stewart platform consisting of a top platform, linear actuators, a bottom platform, spherical joints, and universal joints - Modified from Mura (2011).

The Stewart platform is a parallel-link mechanism, which refers to the parallel structure of the actuators connecting the two platforms (Figure 3.4). The main features of the structure are high rigidity, precision, and load capacity (Mura 2011). Due to these advantages of the Stewart platform, it has been applied in several applications, such as precision manipulators, radio telescope orientation, aircraft simulators and rehabilitation devices (Torii et al. 2012, Su et al. 2003, Nanua et al. 1990).

Although the Stewart platform has many advantages, it also possesses some disadvantages including heavy-weight and complex kinematic and dynamic analyses due to the configuration (Dasgupta & Mruthyunjaya 2000).

3.3.1.1 Position of joints

The parallel structure of the Stewart platform causes a symmetrical distribution of joints (Becerra-Vargas & Morgado Belo 2012). Figure 3.5 shows a 2D illustration of a circular shaped top and bottom platform

having six points representing six different joint positions.

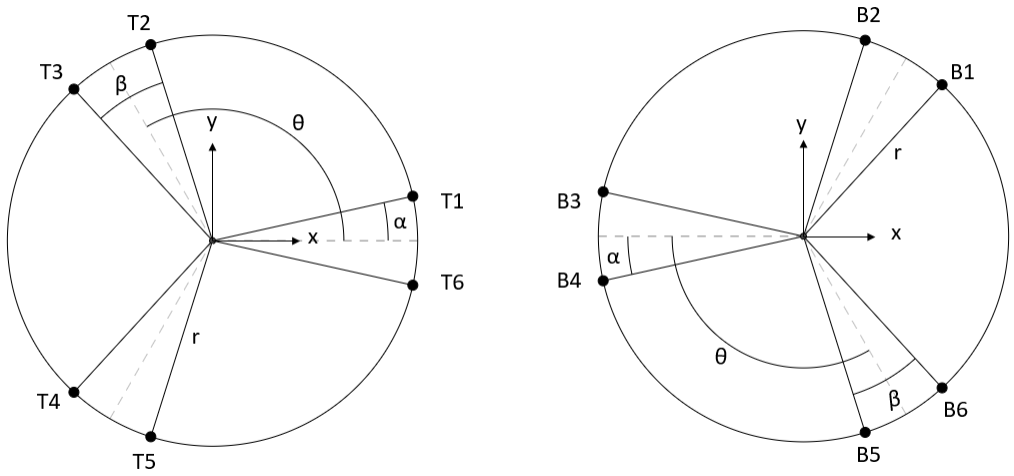

Figure 3.5: Left: The top platform including three joint pair positions (T1 and T6, T2 and T3, and T4 and T5) seperated by an angle, θ. Each joint pair is seperated by an angle of 2· α=β. Right: the bottom platform including three joint pairs (B1 and B2, B3 and B4, and B5 and B6). The position of the joints are separated by the same angles as the joints on the top platform.

The symmetrical distribution of the joints entails that a joint pair (i.e. T1 and T6) is positioned θ =120° apart from another joint pair (i.e. T2 and T3). Each joint is then located at α on each side of θ. Thus, the joints in a joint-pair will be separated by 2 α = β. When the circle has a radius r, the (x, y) coordinates of the six points T1, T2, T3, T4, T5 and T6 located on the top platform can be calculated:

$$T1 = (r \cdot \cos(\alpha), r \cdot \sin(\alpha)) \tag{3.1}$$

$$T2 = (r \cdot \cos(\theta - \alpha), r \cdot \sin(\theta - \alpha)) \tag{3.2}$$

$$T3 = (r \cdot \cos(\theta + \alpha), r \cdot \sin(\theta + \alpha)) \tag{3.3}$$

$$T4 = (r \cdot \cos(2 \cdot \theta - \alpha), r \cdot \sin(2 \cdot \theta - \alpha)) \tag{3.4}$$

$$T5 = (r \cdot \cos(2 \cdot \theta + \alpha), r \cdot \sin(2 \cdot \theta + \alpha)) \tag{3.5}$$

$$T6 = (r \cdot \cos(3 \cdot \theta - \alpha), r \cdot \sin(3 \cdot \theta - \alpha)) \tag{3.6}$$

The coordinates of the six points B1, B2, B3, B4, B5 and B6 located on the bottom platform, can also be calculated, as the points are located opposite compared to the top platform.

$$B1 = (r \cdot \cos(0.5 \cdot \theta - \alpha), r \cdot \sin(0.5 \cdot \theta - \alpha)) \tag{3.7}$$

$$B2 = (r \cdot \cos(0.5 \cdot \theta + \alpha), r \cdot \sin(0.5 \cdot \theta + \alpha)) \tag{3.8}$$

$$B3 = (r \cdot \cos(1.5 \cdot \theta - \alpha), r \cdot \sin(1.5 \cdot \theta - \alpha)) \tag{3.9}$$

$$B4 = (r \cdot \cos(1.5 \cdot \theta + \alpha), r \cdot \sin(1.5 \cdot \theta + \alpha)) \tag{3.10}$$

$$B5 = (r \cdot \cos(2.5 \cdot \theta - \alpha), r \cdot \sin(2.5 \cdot \theta - \alpha)) \tag{3.11}$$

$$B6 = (r \cdot \cos(2.5 \cdot \theta + \alpha), r \cdot \sin(2.5 \cdot \theta + \alpha)) \tag{3.12}$$

This geometry will ensure a symmetrical distribution of the joints, where the actuators are connected to the platforms, and a symmetrical distribution of the load applied to the platform. (Becerra-Vargas & Morgado Belo 2012)

3.3.1.2 Linear actuators

The components connecting the platforms are linear actuators which are the drivers in a Stewart platform. Actuators can be driven by pressurised air (pneumatic), fluid (hydraulic) or electricity (electric) to create a linear motion or force. (Craig 2005)

Pneumatic linear actuators

These actuators consist of a piston encased in a hollow cylinder. Pressure from external compressors or a manual pump makes the piston move linear to the cylinder. The advantages of pneumatic actuators are simplicity, accuracy, lightweight, and sustainability in extreme temperatures. Disadvantages include a constantly running compressor, even in static extended positions and the need for oil and lubrication, causing downtime. (Craig 2005)

Hydraulic linear actuators

Hydraulic actuators work similarly as the pneumatic actuators. The main difference is that the piston is moved by incompressible liquid from a pump rather than pressurised air. The advantage of hydraulic actuators is their suitability in high-force applications. They can produce roughly 25 times more force than pneumatic actuators of equal size and do not need the pump to supply fluid to maintain an extended position. Accommodation of the hydraulic actuators may be difficult due to the need of the major parts, including fluid tank, motors, pumps, heat exchangers, etc. (Craig 2005)

Electric linear actuator

The electric actuator converts electrical energy into motion by a torque. A mechanically connected electric

motor turns a lead screw to create linear motion. Electric actuators offer the best precision-control positioning and a scalability of force requirement making them suitable for most purposes. Besides, the noise level is lower compared to the pneumatic and the hydraulic actuators. Furthermore, in contrast to the pneumatic and hydraulic actuators, the actuators cannot leak. Disadvantages with the electric actuators are the high price, environmental sustainability and a continuously running motor that may lead to overheating of the device. (Craig 2005)

Positioning of linear actuators

Linear actuators can be embedded with sensors which provide direct control between the stroke position and the control system. This function is critical in complex actuator systems as it allows the system to memorise settings and the user can monitor the stroke lengths at all times. Typical position sensors are Hall effect sensors and potentiometers. Hall effect sensors are based on a change of a magnetic field when the actuator is extended or retracted. The magnetic field is converted into a voltage signal by the sensor, subsequently used for position feedback. Potentiometers are the most common sensor in the industrial market. The positioning is controlled by a proportional relationship between an electrical output generated by the distance between two contacts. As the screw turns and the actuator is extended or retracted the electrical output changes. (Mueller & Rosenfeld 2017)

3.3.1.3 Kinematics and dynamics of a Stewart platform

Kinematics and dynamics are important factors in a high precision application of Stewart platforms as model simplifications, and complex algorithms can lead to decreased precision and accuracy (Dasgupta & Mruthyunjaya 2000). Typically, the kinematics of the Stewart platform can be divided into inverse kinematics and forward kinematics. The forward kinematic solution involves calculations to find the position and orientation of the top platform from the length of each actuator (Ghobakhloo et al. 2006, Schipani & Marty 2006, Becerra-Vargas & Morgado Belo 2012). These calculations can be very complicated and difficult to solve as they require the solution of multiple non-linear equations (Dasgupta & Mruthyunjaya 2000, Charters et al. 2009). Furthermore, forward kinematics often results in more than one solution, leading to multiple positions for the top platform can be calculated from a specific combination of actuator lengths (Charters et al. 2009). The inverse kinematics is more straightforward as deriving the equations is easier compared to the forward kinematics (Charters et al. 2009). Figure 3.6 shows a diagram of the points used to calculate the actuator length based on a desired position and orientation of the top platform.

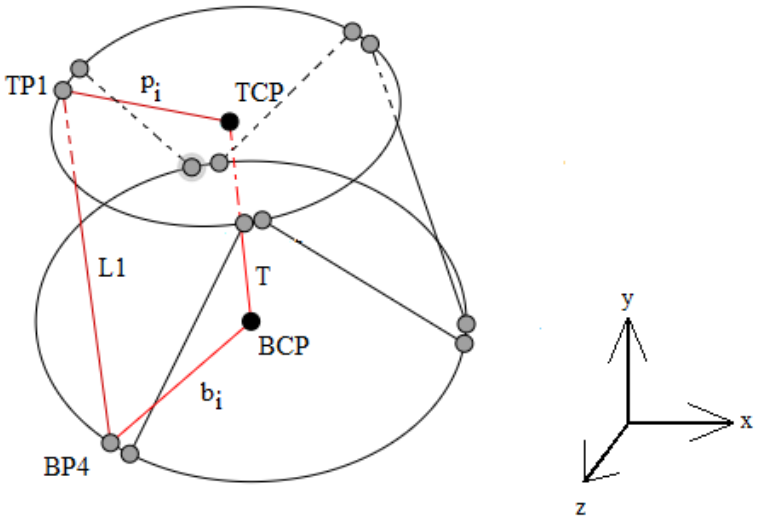

Figure 3.6: Diagram of kinematics involved in the inverse kinematics of a stewart platform, including a joint position on the top platform (TP1), a joint position on the bottom platform (BP4), a centre point on the top platform (TCP), a centre point on the bottom platform (BCP), a vector from BCP to BP4 (b_i), a vector from TCP to TP1 (P_i), a vector from BCP to TCP (T), and a vector between BP4 and TP1 (L1).

Vector $\vec{p_i}$ and $\vec{b_i}$ are the centre point coordinates of the top (TCP) and bottom platform (BCP) to the joints TP1 and BP4, respectively. The vector, $\vec{T}$, represents a linear displacement of the TCP with respect to the coordinate system of BCP. This geometrical relation can be used to calculate the length of an actuator based on a specific position and orientation of the top platform (Dasgupta & Mruthyunjaya 1998). In the following equation, the length of an actuator (L_1) is calculated by:

$$L_1 = T + R \cdot \vec{p_i} - \vec{b_i} \tag{3.13}$$

The orientation of the top platform can be determined by multiplying the coordinates of 'p_i' with a rotation matrix 'R', translating the position of the joint 'TP1' into the coordinate system of the bottom platform (Bingul & Karahan 2012). 'R' is given by:

$$R = \begin{bmatrix} cos\psi cos\theta & -sin\psi cos\phi + cos\psi sin\theta sin\phi & sin\psi sin\phi + cos\psi sin\theta cos\phi \\ sin\psi cos\theta & cos\psi cos\theta + sin\psi sin\theta sin\phi & -cos\psi sin\phi + sin\psi sin\theta cos\phi \\ -sin\theta & cos\theta sin\phi & cos\theta cos\phi \end{bmatrix} \tag{3.14}$$

In equation (3.14) 'ϕ', 'θ', 'ψ' are the rotations around the x, y, and z-axis, respectively (Bingul & Karahan 2012).

Summarised, the inverse kinematics solution can be described as the calculation of each actuator length from a given position and orientation of the top platform (Nair & Maddocks 1994, Schipani & Marty 2006).

The dynamics of a Stewart platform can also be divided into two principles: forward and inverse dynamics (Bingul & Karahan 2012). Forward dynamics involves calculations of the top platform trajectory (position, velocity and acceleration) from a given set of actuator forces. The inverse dynamics calculates the necessary actuator forces to generate a given top platform trajectory (Lopes 2009). During the last decades, researchers have investigated the dynamics of a Stewart platform by different methods, such as the Newton-Euler method, the Lagrange formulation, the principle of virtual work, etc. (Bingul & Karahan 2012). The Newton-Euler method requires calculation of all forces and moments between the joints (Dasgupta & Mruthyunjaya 1998). The Lagrange formulation tries to describe the dynamics of the system from the theory of work and energy (Abdellatif & Heimann 2009). The main reason to approach the dynamics of the Stewart platform by different methods is to minimise the number of calculations and computational load (Dasgupta & Mruthyunjaya 2000, Bingul & Karahan 2012).

3.4 EOS X-ray scanner

A common way of modern particle detection is by measurements of ionisation, which is the number of electrons separated from atoms after a collision with elemental particles (for example, X-ray's photons). This method significantly reduces the affection of radiation exposure while improving the quality of captured x-ray images. Thus, images of higher quality with a wider dynamic range, resulting in images with distinct grey shades increased to 30-50 thousand as opposed to traditional X-ray images with only a few hundred grey shades. Furthermore, the image pixel resolution is improved regarding sharpness and contrast. (Illés & Somoskeöy 2012)

3.4.1 Principles of the EOS X-ray scanner

The EOS X-ray scanner is the first X-ray scanner where this new technology is incorporated. The technology is based on Charpak's multiwire proportional chamber theory, where the Charpak's chamber is placed between a radiographed object and a distal detector (Figure 3.7). Because of this, the EOS scanner can use a very small dose of radiation while still producing a high-quality X-ray image. (Wybier & Bossard 2013, Illés & Somoskeöy 2012)

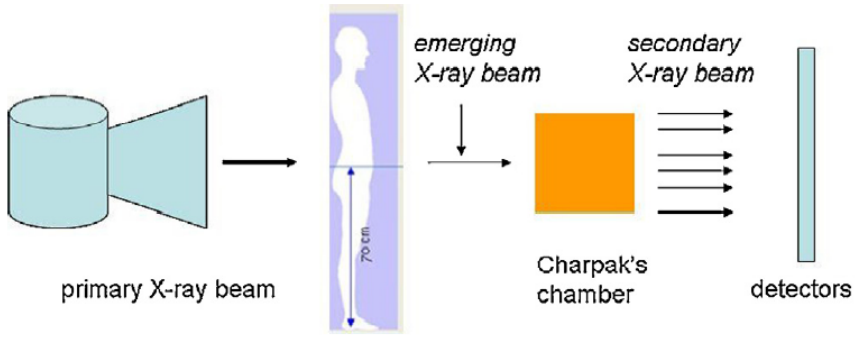

Figure 3.7: Illustrative representation of the EOS X-ray scanner with the Charpak's chamber - Modified from Wybier & Bossard (2013).

The scanner consists of two orthogonally co-linked pairs of 450 mm wide linear radiation sources and detectors; one frontal and one lateral (Figure 3.8). These X-ray tubes capture either uni- or biplanar images with the biplanar being spatially calibrated simultaneously. The detectors can cover an area with a height of 1800 mm and a width of 450 mm, thereby creating a high quality, high contrast anteroposterior and lateral X-ray image in up to 45 seconds. (Illés & Somoskeöy 2012)

Figure 3.8: Left: The EOS X-ray scanner. Middle: the co-linked linear radiation sources and detectors. Right: A 3D-reformatted model - Modified from Illés & Somoskeöy (2012).

A three-dimensional (3D) reconstruction of specific parts of the skeletal system can be created from the frontal and lateral two-dimensional (2D) images captured by the EOS X-ray scanner (Figure 3.8). This virtual and generic reconstruction process involves comparison of 3D computed tomography (CT) models and comparison of specific points on the bone surface, and depending on the complexity of the bone structure the number of points to accurately describe a 3D envelope varies from 400 to 9000. The virtual bone shapes of the 3D CT models are obtained from a 3D model repository, created from 1628 individuals and statistical finite element models. (Wybier & Bossard 2013)

3.4.2 Practical implications

The new technology used in the EOS X-ray scanner was firstly intended to solve two main problems:

1. Determination of individual spinal vertebrae positions in the axial plane. This can be attained through the new 3D reconstruction of frontal and lateral 2D pictures e.g. creating a high-quality image of the pelvic girdle which could not be done with conventional X-ray technology.
2. Reduction of the current radiation dose. The new technology could reduce radiation to one thousandth compared to the CT 3D method, and six to nine times lower compared to regular digital radiography. (Wybier & Bossard 2013)

The 3D reconstruction from the EOS software can be used for recognising and matching specific reference points as well as detecting and displaying different bone contours through the co-paired X-ray tubes. The EOS scanner has been proven to be as accurate and applicable as the 3D CT method, using 800-1000 times less radiation in comparison. Thus, the ability to produce a directly applicable high-quality full-body digital X-ray image within 45 seconds, while maintaining radiation to a minimum, is an important practical application. Furthermore, the EOS allows for X-ray images in a 1:1 scale, making further processing easier for examiners. Thus, the EOS X-ray scanner allows physicians to create a 3D reconstruction and visualisation of an individual, thereby enabling analysis of relative joint and ligament position and orientation. Furthermore, the scanner can be used to examine the volume, lengths, angles of extremities, axial rotation and torsion of segments, as well as a single joint under physiological load. (Illés & Somoskeöy 2012)

One of the main limitations of the EOS X-ray scanner is movement artefacts during scanning. Patients are usually asked to stand in an upright position, in the centre of the scanner, which can cause movements in vague patients such as children or elderly. Several precautions have been made, including creating a device to help sustain the position in the upper limbs. Furthermore, for uniplanar X-rays, patients are asked to stand upright against the suitable wall of the scanner. (Wybier & Bossard 2013)

3.4.3 3D knee laxity measurements

Measurements of the lower limbs have been improved with the EOS X-ray scanner technology, leading to goniometry being conducted with EOS images. Through calibrated frontal and lateral images of the lower limbs, examiners can measure integrated values of the angles in 3D-reformatted images of femur and tibia. Although clinicians are used to examining conventional 2D images of in particular knee frontal deformation,

the 3D EOS images may be different in comparison. Thus, it would still be necessary to provide 2D images together with the EOS images until clinicians become familiar with the new technology. (Wybier & Bossard 2013)

To examine static knee joint laxity, the ligaments of the knee joint needs to be stressed individually or simultaneously (Section 3.1.2.1). Furthermore, (Pedersen et al. 2017) used a low-dose X-ray scanner in combination with 3D image data reconstructed from CT scans, to investigate tibia displacement relative to the femur. This was done by segmenting tibia and femur to reconstruct the 3D bone geometries onto the biplanar low-dose x-ray images. The position and orientation were found by an iterative approach, matching the closest point between contours of the low-dose x-ray images and the projected contours from the 3D image data. A proof-of-concept test showed that this method is capable of obtaining the amount of static knee joint laxity.

Concept development 4

This chapter aims to give a progressive description of the process and considerations involved in the development of a six DOF arthrometer for static examination of knee joint laxity. The process was initiated by defining user needs and specific product requirements based on the current problems within static knee joint laxity examinations. Lastly, a description of the conceptual idea and a brief delimitation of the thesis will follow.

4.1 Product requirements

During product development, several considerations should be taken into account before manufacturing of the product. These should include reflections regarding user needs and how these can be translated into specific product requirements. (Ulrich & Eppinger 2004)

4.1.1 Current problems

The theory outlines several limitations of the current examination procedures of static knee joint laxity (Section 3.1). The following issues summarise the problems regarding physical methods by clinicians:

- Inter-examiner subjectivity - The quality of the current examination procedures depends mainly on the experience of the clinician, due to bias from limited standardisation which entails a poor reliability (Scholten et al. 2003, Mouton et al. 2012).
- Non-quantifiable - Inexact measurements may cause limited ability to compare results between clinicians (Musahl et al. 2017).

A similar assessment of arthrometers showed:

- One-dimensionality - Single-plane arthrometry is currently the only commercially available type of measurement device to document static knee joint laxity. Multiple plane arthrometry is needed in

conjunction with physical examinations to understand the injury fully. (Musahl et al. 2017)

- Soft tissue artefacts - Skin movement across the medial and lateral femoral condyles may affect the accuracy of non-invasive examination results (Musahl et al. 2017).
- Objectivity - Although arthrometers provide clinicians with feedback related information regarding the amount of force applied, the rate of the force is personalised. The result lacks reliability similar to the physical examinations. (Branch et al. 2010).

4.1.2 User needs

The development of a new arthrometer needs to accommodate the current problems to permit measurement of static AP, VV, and IE knee joint laxity. Therefore, when translating the current problems into user needs, the arthrometer needs to enable:

1. Mobility, allowing static AP, VV, and IE laxity examinations, accordingly.
2. A load capacity allowing static AP, VV, and IE laxity examinations, accordingly.
3. Displacement of the tibia relative to the femur.
4. Objective quantification of knee joint laxity.

4.1.3 Specific product requirements

The user needs can be translated into specific product requirements:

1. Mobility, allowing static AP, VV and IE laxity examinations accordingly.
    - A translation of 11.4 $\pm$ 2.9 mm in the sagittal plane (AP).
    - A rotation of 20.1 $\pm$ 6.4° in the frontal plane (VV).
    - A rotation of 27.8 $\pm$ 7.6° in the transverse plane (IE).
2. A load capacity allowing static AP, VV and IE laxity.
    - Load the knee with 134 N during AP tests.
    - Load the knee with 22.1 Nm during VV tests.
    - Load the knee with 5 Nm during IE tests.

3. Displacement of the tibia relative to the femur.
    - Fix the tibia to the arthrometer.
    - Fix the thigh externally.
4. Objective quantification of knee joint laxity.
    - Measurement of in vivo knee joint laxity.

The amount of translation and rotation is based on previous literature examining knee joint laxity (Section 3.1).

4.2 Conceptual idea

To comply with the specific product requirements, it is necessary to consider the requisite product requirements (Ulrich & Eppinger 2004).

By incorporating a parallel-link mechanism, the arthrometer would be able to move in six DOF (three translational and three rotational) and thereby cope with the movements needed for the AP, VV, and IE knee joint laxity tests (Section 3.3). Thus, the mobility of the arthrometer enables the movement used for static examination of knee joint laxity.

Although the movement might be secured this way, the load capacity of the arthrometer needs to be in agreement with the current examinations. If the arthrometer is not able to produce enough force, the ligaments will not be stressed accordingly, thus, the result of the examination will be affected. Additionally, if the arthrometer is incapable of inducing force in the proper location of the knee, the chance for erroneous examination results increases. By including a standardised and controlled examination protocol along with a targeted component selection these issues could be resolved.

Standardisation - For a standardisation of the force, the tibia and femur need to be fixated to displace the tibia relative to the femur. Thus, by attaching an aircast boot to the top platform of the arthrometer and deploying a chair-like structure with a strap, fixation points of the tibia and femur could be determined. This solution might ensure movement of the arthrometer to directly affect the tibia while femur remains in a secured position.

Force control - To comply with the loads during the knee joint laxity examinations, the arthrometer needs to be able to measure the amount of force acting on the top platform. This can be achieved by incorporating a force sensor which enables measurements and recordings of forces and moments acting translationally and

rotationally. By creating a force feedback loop, the arthrometer would be able to induce the correct amount of force without risking injury of the subject. When the required force or moment is reached e.g. 134 N during AP examination, the platform should stop moving.

Material selection - If the arthrometer should be capable of producing a predetermined amount of force, each actuator in the parallel-link mechanism needs a certain load capacity and positional control. Linak produces innovative electric actuator systems for the purpose of "improving people's quality of life and working environment" (Linak 2017). Linak has previously shown the willingness to cooperate with students, and with internal values committing to innovation, individual efficiency, always being at the cutting edge of the market, and openness to new challenges and opportunities, the company would be a perfect fit for cooperation.

The product properties described are capable of stressing the ligaments according to the procedures of static knee joint laxity examinations, however, it cannot measure the amount of laxity. To cope with the specific product requirement of being able to measure knee joint laxity, several methods could be considered.

Forward kinematics - By using forward kinematics, it is possible to quantify the displacement of the top platform relative to the bottom platform in a static position by the length of each actuator (Ghobakhloo et al. 2006). This could be used to calculate the amount of static knee joint laxity, however, the approach is based on complicated calculations and can be influenced by external factors, such as soft tissue artefacts.

3D imaging - The EOS X-ray scanner provides the opportunity to scan and create a 3D-reformatted image of the femur, tibia, and knee joint, through calibrated frontal and lateral images (Section 3.4). By implementing the method of (Pedersen et al. 2017), the amount of static knee joint laxity can be determined by placing the arthrometer in an EOS X-ray scanner and stressing the ligaments. By this approach, it would be possible to measure non-invasive in vivo static knee joint laxity and thereby limit the influence from skin artefacts.

4.2.1 Final design

From the conceptual idea, the final design was chosen to consist of a six DOF arthrometer constructed by a top and bottom platform connected by six linear actuators from Linak. An aircast boot should be attached on the top platform of the arthrometer connected by a force sensor (Figure 4.1).

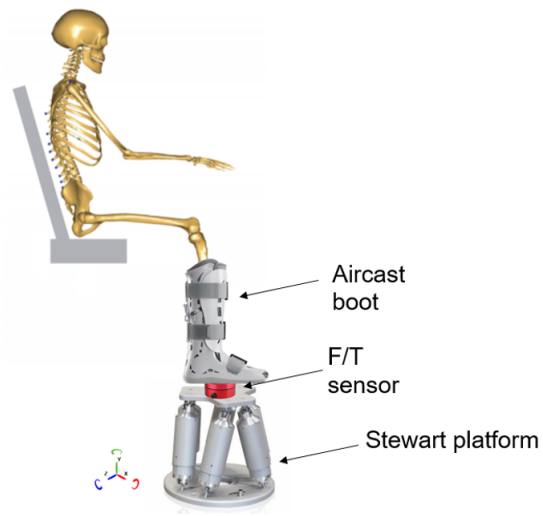

Figure 4.1: The conceptual idea including a Stewart platform, a force sensor, and an aircast boot.

The arthrometer should be used in collaboration with a chair-like structure fixating the thigh, and both should be able to fit inside an EOS X-ray scanner. This setup allows clinical loads to be applied while biplanar X-ray images are captured. Using the method of Pedersen et al. (2017), the amount of static knee joint laxity can be determined.

The current thesis focused on the development of the arthrometer. No further considerations regarding the chair structure, the aircast boot, and the force sensor will be included.

Arthrometer development 5

The following chapter includes calculations regarding the dimensions and range of motion (ROM) of the arthrometer and AMS simulations for size determination of the linear actuators and platforms. Furthermore, a description of the processing of the simulation results, which leads to a determination of platform dimensions and actuator type.

5.1 Calculations of range of motion and load capacity

The length and load capacity of the linear actuators are related to the movements performed in a static knee joint laxity examination since the actuators execute the movements. Because of this, the required ROM and load capacity of the arthrometer need to be determined in advance.

To ensure the necessary ROM and load capacity of the arthrometer, calculations based on the highest values from the previous literature were conducted (Section 3.1.2.1). Two times the standard deviation were added to ensure a testing capability of 95 % of a normally distributed population (Zar 2010). In addition, a buffer of 25 % was added to this value. Therefore, the ROM and load capacities were calculated as follows.

5.1.1 Anterior-posterior laxity

Ganko et al. (2000) reported AP laxity values of 11.4 mm ± 2.9 mm, examined using the KT-1000 arthrometer. With these values the arthrometer should be able to move:

$$(11.4\mathrm{mm} + 2 \cdot 2.9\mathrm{mm}) \cdot 1.25 = 21.50\mathrm{mm} \tag{5.1}$$

Therefore, the AP ROM of the platform should be 21.5 mm. Furthermore, AP laxity was examined using a force of 134 N. When including a buffer of 25 % the arthrometer should be able to push 167.5 N.

5.1.2 Varus-valgus laxity

Creaby et al. (2010) reported VV laxity values of 20.1° ± 6.4°. This value was the total VV laxity from maximum varus to maximum valgus. Assuming that the laxity value was equal in varus and valgus, the total value is split in two. Therefore, with these values the arthrometer should be able to move:

$$\frac{20.1° + 6.4° \cdot 2}{2} \cdot 1.25 = 20.56° \tag{5.2}$$

Therefore, the VV ROM should be 20.56° in both varus and valgus rotation. Furthermore, the laxity was examined using a torque of 22.1 Nm. Including 25 %, the arthrometer should be able to create of torque of 27.63 Nm.

5.1.3 Internal-external laxity

Schultz et al. (2012) reported IE laxity values of 27.8° ± 7.6°. This value was the total IE laxity. Assuming an even amount of internal and external laxity, the total value was split in two. Hence, the arthrometer should be able to rotate:

$$\frac{27.8° + 7.6° \cdot 2}{2} \cdot 1.25 = 26.88° \tag{5.3}$$

Therefore, of IE ROM was 26.88° in both internal and external rotation. Furthermore, the laxity was examined using a torque of 5 Nm. Including a 25 % buffer, the arthrometer should be able to create a torque of 6.25 Nm during IE rotation.

These values represent the ROM and load capacity for the arthrometer. However, the ROM depends on the length of the knee height, e.g. a person with a longer lower leg would require a larger movement to create a VV rotation of 20.5°. To account for this, a knee height of 0.55 m was implemented to make sure, that the arthrometer would be able to examine 95 % of people. The knee height was based on an anthropometric study (Harrison & Robinette 2002), which shows that 95 % of a normally distributed population has a knee height of 0.55 m or lower.

5.2 Arthrometer size

To determine the size of the arthrometer, the dimensions of the EOS X-ray scanner and human anthropometrics was considered. Therefore, calculations regarding the size of the arthrometer were conducted to make sure it would fit within the area. Calculations were based on being able to examine 95 % of a normally distributed population. The anthropometric measures used for the calculations are listed in Table 5.1.

Table 5.1: Anthropometric values of knee height, buttock-knee length, sitting height, and knee flexion angle for 95 % of a normally distributed population (Harrison & Robinette 2002).

Measure	**Abbreviation**	**Value**
Knee height	KH	55 m
Buttock-knee length	BK	0.673 m
Sitting height	SH	0.985 m

A simplified drawing of a person with these anthropometric measures, within the EOS X-ray scanner, was created (Figure 5.1).

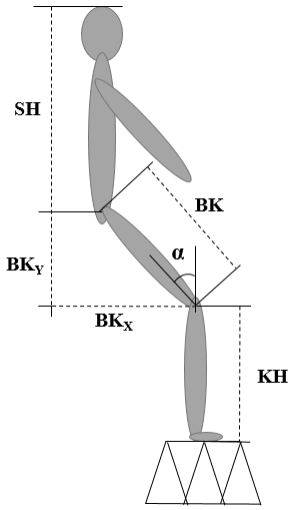

Figure 5.1: The set up used for calculating the remaining horizontal and vertical space within the EOS X-ray scanner. SH = Sitting height, BK_Y = vertical Buttock-knee length, BK_X = horizontal Buttock-knee length, BK = Buttock-knee length, α = Knee flexion angle, and KH = Knee height.

From Figure 5.1 it can be reasoned that the only dimensions affecting the width, is the BK_X, while SH, BK_y, and the KH are the only dimensions affecting the height, assuming that the lower leg is attached in a vertical position at the centre of the arthrometer. Therefore, calculations of the horizontal and vertical space within the scanner were calculated by using trigonometry:

$$BK_x = \cos(90^\circ - \alpha) \cdot BK \tag{5.4}$$

$$H = SH + KH + (\sin(90^\circ - \alpha) \cdot BK) \tag{5.5}$$

Several researchers have previously used arthrometers with a knee flexion angle (α) of 20° to 90° to investigate static knee joint laxity (Musahl et al. 2017). Thus, equation (5.4) and (5.5) and knee flexion angles ranging from 20° to 90°, were used to calculate the horizontal and vertical dimensions of a person in the scanner. The values were subtracted from the height (2700 mm) and width (760 mm) of the EOS X-ray scanner,

assuming the arthrometer is not restricted by any obstacles inside the scanner. This was done to estimate the maximum radius and height of the arthrometer.

Table 5.2: Maximum radius and height of the arthrometer, with angles ranging from 20° to 90°.

Angle [°]	**Radius** [mm]	**Height** [mm]
90	87.00	1165.00
80	97.22	1048.13
70	127.59	934.82
60	177.16	828.82
50	244.45	732.40
40	327.40	649.45
30	423.50	582.16
20	529.82	532.59

From Table 5.2 it can be seen that as the knee flexion angle increases, the height increases as well but the radius decreases. However, as the width of the EOS X-ray scanner is 760 mm, the radius of the top and bottom platform of the arthrometer can be 380 mm maximum.

5.2.1 Considerations regarding dimensions and ROM

The radius and height of the arthrometer were calculated in a static position. However, as the arthrometer should be capable of performing the movements involved during AP, VV, and IE laxity examinations of static knee joint laxity, additional calculations, incorporating the ROM of the arthrometer were conducted.

The calculation for AP movement is relatively simple, as the displacement is solely translational. Thus, half the AP ROM is subtracted from the maximal radius of the arthrometer. This means that in order to perform the AP static knee joint laxity examination movement, the maximum radius was:

$$R_{max(AP)} = \frac{760mm}{2} - \frac{21.5mm}{2} = 36.93mm \tag{5.6}$$

The maximum angular displacement during a VV knee joint laxity test was used to calculate the maximum radius ($R_{max(VV)}$) of the arthrometer, without bumping into the wall (Figure 5.2):

$$D_x = \sin(\alpha) \cdot KH = \sin(20.5°) \cdot 550mm = 192.61mm \tag{5.7}$$

$$R_{max(VV)} = \frac{\frac{EOS_w}{2} - D_x}{\cos(\alpha)} = \frac{\frac{760mm}{2} - 192.61mm}{\cos(20.5°)} = 200.05mm \tag{5.8}$$

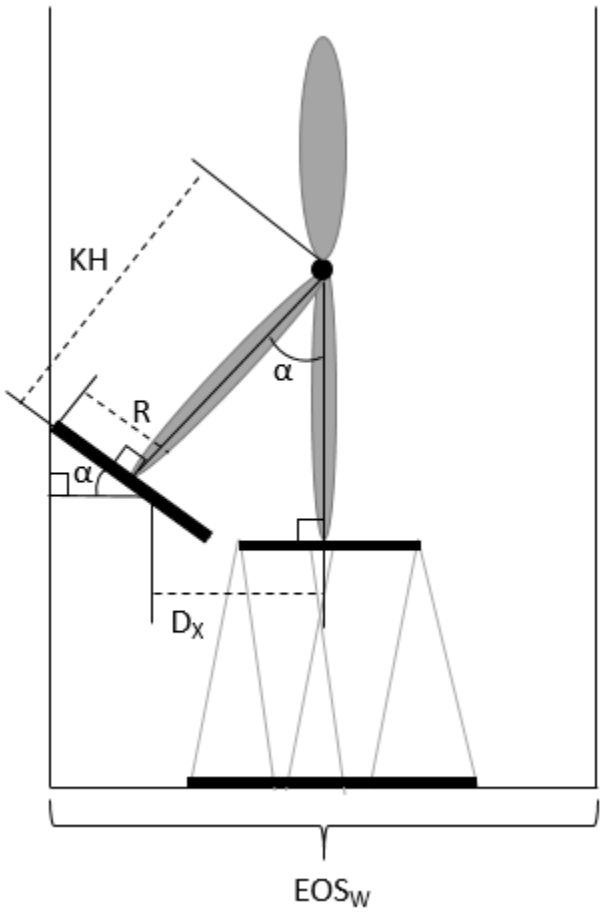

Figure 5.2: Illustration of the dimensions used to calculate the maximum radius of the top platform during VV examination. KH = Knee height, R= radius of the arthrometer, α = VV rotation angle , EOS_W = Width of EOS X-ray scanner, and D_X = horizontal displacement of the top platform.

The movement during the IE examination does not restrict the radius or height of the arthrometer, as it rotates around the vertical axis.

5.2.2 Size limitations for arthrometer

In order to avoid collision with the EOS x-ray scanner, the radius of the arthrometer may not exceed 200.05 mm. Furthermore, the height of the arthrometer could not exceed 530 mm in order to have a knee flexion angle of 20°.

5.3 AnyBody simulations

Computer simulations were computed to estimate the required length and stroke length of the linear actuators to execute the desired movements. However, as the dimensions of the top and bottom platform are unknown,

multiple configurations existed. Thus, an estimation of the top and bottom platform radius and the height between these were requisite.

5.3.1 First model iteration

In the first model the position of the joints was determined to be located 120° apart, due to the compliance of symmetrical distribution (Section 3.3.1.1). Each joint was modelled as an 'AnyRefNode'. The first model iteration was created with the assumption that two actuators are connected at the same joint. Thus, both platforms had three nodes connected with six 'AnyKinPlines' to measure the distance between the nodes (Figure 5.3).

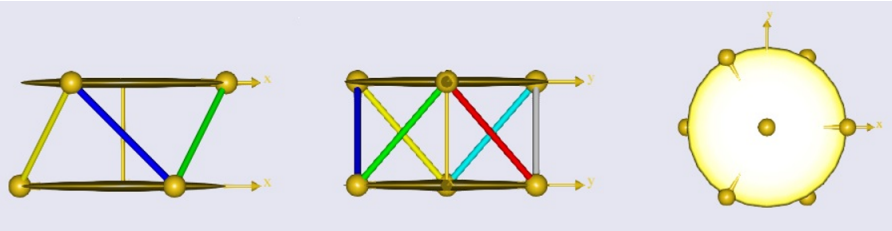

Figure 5.3: The first design model iteration. Left: Top view. Middle: Frontal view. Right: Lateral view.

The first iteration was a simplification of a Stewart platform (Section 3.3.1). However, the theory of Stewart platforms outlines that six attachment points are needed. In addition, as the first model iteration leaves no room for joints for mounting the linear actuators, the simplifications might lead to inaccurate estimations. As a consequence, a more detailed model of the Stewart platform was created.

5.3.2 Second model iteration

A second model iteration, with six nodes on each platform, was modelled. This was done by separating the nodes by an angle of 12.5° on each side of the original position, thereby, separating two nodes in a joint pair by 25°. (Section 3.3.1.1). Furthermore, the attachment points of the top and bottom platform were repositioned 20 mm below and above, respectively, to account for the connecting joints (Figure 5.4).

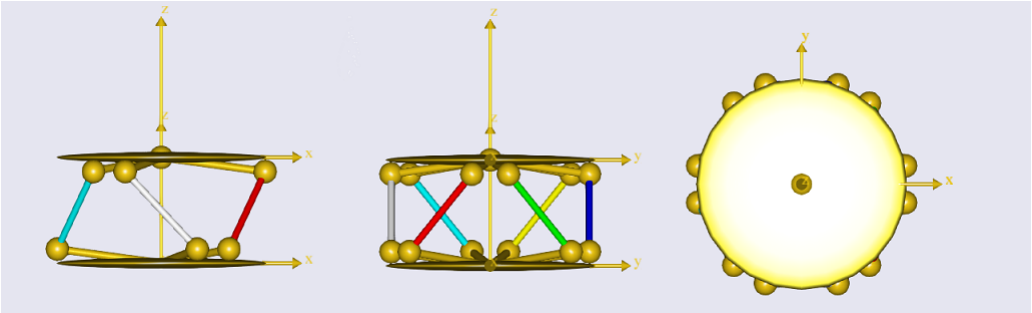

Figure 5.4: The second design model iteration. Left: Top view. Middle: Frontal view. Right: Lateral view.

The second model iteration was used to simulate the movement of the arthrometer during AP, VV, and IE examinations of static knee joint laxity.

5.4 Parameter study

As VV and IE laxity are described as angular displacements rather than a translative displacement, the knee height was modelled as a line on the top platform and assigned as the driver for the movements. However, as the length of the knee height affects the movements, it was ensured that individuals with a long lower leg would be able to be tested. As described in the calculations regarding the size of the arthrometer, a lower leg length of 0.55 m was used.

5.4.1 Boundary conditions

The boundary conditions for the top (TP_r) and bottom platform radius (BP_r) were set by the size calculations of the arthrometer (Section 5.2). The minimum and maximum radius for the top and bottom platform was determined to be 100 mm and 200 mm, respectively. The minimum and maximum distance between the platforms (height) was determined to be 100 and 500 mm, respectively.

To investigate the radius between 100 mm and 200 mm, five simulations were conducted in the AMS in steps of 25 mm (Table 5.3). For the height of the arthrometer, nine simulations were carried out in the AMS, in steps of 50 mm between 100 and 500 mm (Table 5.3).

Table 5.3: Potential configurations of the top platform radius (TP_r), the Bottom Platform radius (BP_r), and height of the arthrometer

TP_r [mm]	BP_r [mm]	Height [mm]
100	100	100
125	125	150
150	150	200
175	175	250
200	200	300
		350
		400
		450
		500

5.4.2 Laxity tests

The AP, VV, and IE movements were calculated in Section 5.1 and these values were used as the input for further testing (Section 5.1).

5.4.2.1 Anterior-posterior

The AP test was performed by alternately moving the top platform 21.5 mm in the X and Y axes (Figure 5.5). The X and Y axes were investigated in the positive and negative directions, which means that a total of four parameter studies were performed for the AP test. During the simulations, a force of 167.5 N was applied to the top platform in the opposite direction to represent the reaction force of the knee joint during AP examination (Section 3.1.2.1).

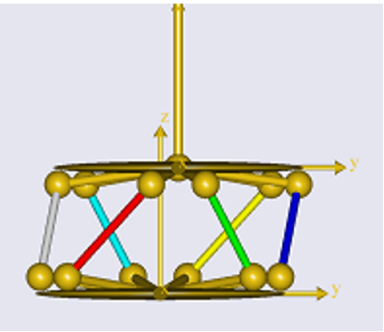

Figure 5.5: The end position of the top platform during the anterior-posterior test.

5.4.2.2 Varus-valgus

The VV test was performed by rotating the top platform 20.5° around the X and Y axes of the knee in both the positive and negative directions (Figure 5.6). During the simulations, a force of 27.63 Nm was applied on the top plate in the opposite direction to simulate the VV laxity test (Section 3.1.2.1). In total, four simulations were performed for the VV test.

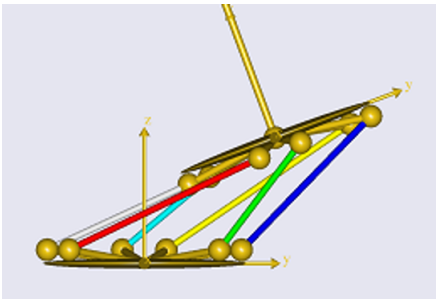

Figure 5.6: The end position of the top platform during the varus-valgus test.

5.4.2.3 Internal-external

The IE test was conducted by rotating the top platform 26.88° around the Z axis in both directions , hence, two simulations were performed for the IE test (Figure 5.7). During the simulations, a moment of 6.25 Nm was applied around the Z axis in the centre of the top platform to simulate the IE laxity tests (Section 3.1.2.1).

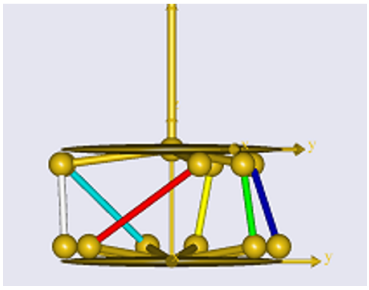

Figure 5.7: The end position of the top platform during the internal-external test.

5.4.2.4 Output of interest

The output of interest from the three laxity tests was chosen to be the minimum and maximum dimensions of the 'AnyKinPline' and the maximum force from each simulation (Section 3.2.1). From this, the stroke length, built-in-dimension (BID), and the relationship between the maximum and minimum 'AnyKinPline' were calculated.

5.5 Selection process

The results from each test were imported into Microsoft Excel 2016 (Microsoft, WA, USA) for a more detailed review. The results consisted of a combination of the load capacity from the AP test, and the minimum and maximum actuator length from the VV test, as it can be reasoned that this test requires the highest ROM (Appendix A.3).

5.5.1 Results and analyses

Due to the limited space, it was preferred to use short linear actuators if possible. The shortest actuator available at Linak is the LA23, which have a minimum BID of 110 mm. In addition, it was preferred that the stroke length should also be relatively small. With this in mind, it was investigated which configurations were possible to use with a BID of 110 mm and a stroke length of 150 mm. With a stroke length of 150 mm, the minimum actuator length (LA_{min}) was 260 mm, and the maximum actuator length (LA_{max}) was 410 mm. To account for the length of the joints mounting the actuators to the platforms an additional 25 mm was added at each end of the actuator (Figure 5.8). With a stroke length of 150 mm, the dimensions of the actuators would be:

$$LA_{min} = 110mm + 150mm + 50mm = 310mm \tag{5.9}$$

$$LA_{max} = 110mm + 150mm + 150mm + 50mm = 460mm \tag{5.10}$$

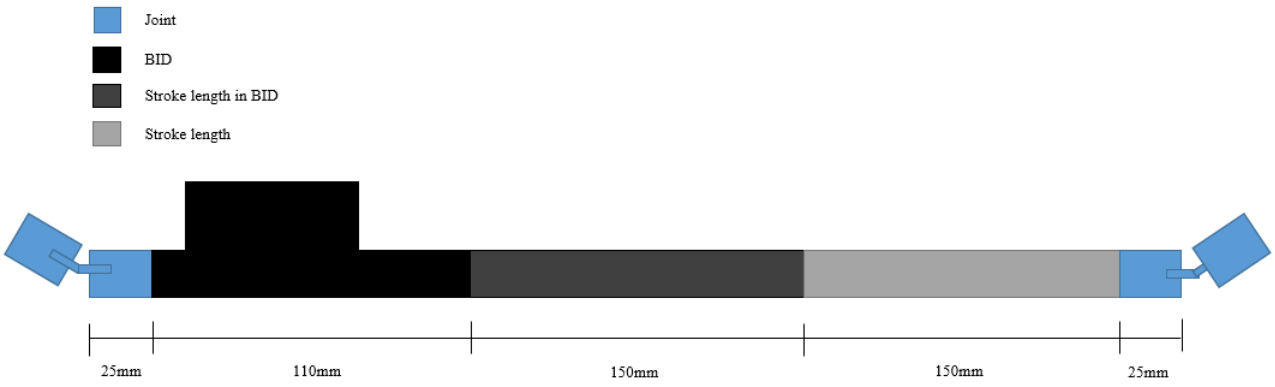

Figure 5.8: The dimensions of the actuator used for sorting out the configurations found in AMS.

Due to the construction of a linear actuator, it was assumed that no actuators are capable of extending more than 1.7 times its original length. Thus, an LA_{min} of 310 mm, LA_{max} of 460 mm, a stroke length

of 150 mm and a relationship of 1.7 was used to sort out configurations which did not comply with these requirements. Hereafter, the number of possible configurations was reduced from 225 to three (Table 5.4).

Table 5.4: The three potential configurations of the AnyBody Modelling System simulations.

Nr.	**TP$_r$** [mm]	**BP$_r$** [mm]	**Height** [mm]	**LA$_{min}$** [mm]	**LA$_{max}$** [mm]	**Stroke length** [mm]	**BID** [mm]	**LA$_{max}$/LA$_{min}$** [NaN]	**Max Force** [N]
15	100	125	350	310.49	446.85	136.36	174.13	1.44	271.91
24	100	150	350	315.86	447.59	131.73	184.13	1.42	228.31
33	100	175	350	319.66	458.38	138.71	180.95	1.43	198.24

From Table 5.4, the best fit was found to be configuration number 15, as this configuration had the smallest BP$_r$, LA$_{min}$, and LA$_{max}$. Thus, the LA23 model from Linak, with dimensions according to configuration 15 was determined to be the preferred actuator model.

5.5.2 Final configuration

Linak was unable to deliver six linear actuators of the preferred model, LA23. Instead of the LA23 model, the company was capable of providing six linear actuators of the model LA12 with an LA$_{min}$ of 255 mm and a stroke length of 100 mm.

To assess whether the LA12 model was a viable option, a new parameter study was conducted in the AMS. As the platforms were already in production, the size of the top and bottom platform had to be predetermined to have a radius of 100 mm and 125 mm, respectively, leaving the height as the only adjustable parameter. The new parameter study was only computed for the VV laxity test, due to the ROM requirement, with heights ranging from 100 mm to 500 mm. Table 5.5 shows the maximum and minimum dimensions of the actuators at nine different heights.

Table 5.5: Results of the new VV test including a buffer of 25% with a top platform and bottom platform of 100 mm and 125 mm, respectively, at nine different heights.

Nr.	**Height** [mm]	**LA$_{min}$** [mm]	**LA$_{max}$** [mm]	**Stroke length** [mm]
1	100	67.59	285.87	218.28
2	150	116.55	305.08	188.53
3	200	165.01	332.56	167.55
4	250	212.81	367.81	155.00
5	300	261.43	406.18	144.75
6	350	310.49	446.85	136.36
7	400	359.79	489.25	129.46
8	450	409.27	532.97	123.70
9	500	458.85	577.71	119.12

Table 5.5 shows that none of the configurations were applicable, as the LA12 have a stroke length of 100 mm. Thus, the buffer of 25% was removed from the ROM values in the parameter study, and a new study was conducted based on the highest values in previous literature (Creaby et al. 2010) (Table 5.6).

$$\mathsf{AP} = 11.4\mathsf{mm} + 2 \cdot 2.9\mathsf{mm} = 17.2\mathsf{mm} \tag{5.11}$$

$$\mathsf{VV} = \frac{20.1^\circ + 6.4^\circ \cdot 2}{2} = 16.45^\circ \tag{5.12}$$

$$\mathsf{IE} = \frac{27.8^\circ + 7.6^\circ \cdot 2}{2} = 21.5^\circ \tag{5.13}$$

Table 5.6: Results of the VV test with top platform and bottom platform of 100 mm and 125 mm, respectively, at nine different heights at a varus-valgus rotation of 16.45°.

Nr.	**Height** [mm]	**LA$_{min}$** [mm]	**LA$_{max}$** [mm]	**Stroke length** [mm]
1	100	67.60	245.63	178.03
2	150	116.55	265.62	149.07
3	200	165.01	294.49	129.48
4	250	212.81	331.12	118.31
5	300	261.43	370.90	108.66
6	350	310.48	412.90	102.42
7	400	359.79	456.51	96.72
8	450	409.27	501.32	92.05
9	500	458.85	547.04	88.19

Table 5.6 showed that no configuration was able to perform the VV laxity test with the dimensions of the LA12. However, configuration number 7, 8 and 9, does not require a stroke length of more than 100 mm. This means that if the LA12 is extended to fit the minimum dimension, it would be capable of performing the VV laxity test. Thus, a linking part was created to extend the configuration to make configuration number eight work. This part also functions as the link between the joints and the actuator.

After receiving the components it was realised, that the dimensions of the actuators and joints were not completely identical as originally assumed. The BID of the actuators is 250 mm instead of the expected 255 mm. In addition, the joints only accounts for 20 mm instead of the expected 25 mm at each end. To account for these deviations, the linking parts was created to extend the actuator by 122 mm (Figure 5.9). Furthermore the arthrometer housing entailed a joint separation of 40° compared to original 25°.

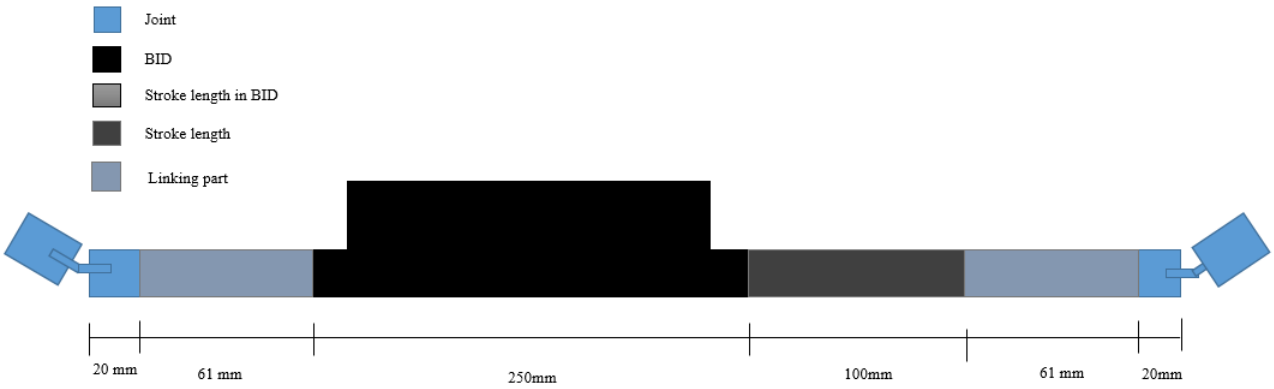

Figure 5.9: The dimensions of the final configuration of the actuators.

Considering these differences between the expected dimensions and the actual dimensions, the shortest and longest arm of the actuator are 412 mm and 512 mm, respectively (Equation 5.14 and 5.15).

$$\mathrm{LA}_{min} = 250\mathrm{mm} + 122\mathrm{mm} + 40\mathrm{mm} = 412\mathrm{mm} \tag{5.14}$$

$$\mathrm{LA}_{max} = 250\mathrm{mm} + 100\mathrm{mm} + 122\mathrm{mm} + 40\mathrm{mm} = 512\mathrm{mm} \tag{5.15}$$

Platform properties 6

The following chapter includes a description of the methods used for a finite element analysis conducted for evaluation of the thickness and strength of the platforms. Afterwards, the results of the test are presented.

From the AMS simulations, the radius of the top and bottom platform was determined. To test the strength of the top platform, a SolidWorks simulation was conducted for the forces acting in the preliminary AMS simulations (Appendix A.5). The bottom platform was not tested, as it is fixed to a solid foundation.

6.1 Finite element analysis

The FEA was conducted in SolidWorks to assess the strength of the top platform during the examination of knee laxity. The analysis was conducted using the highest force from the 15th configuration of the AMS results, 271.91 N (Appendix A.5). From the FEA, the Von Mises stress, displacement, and factor of safety of the top platform were estimated.

Due to limited availability, the material of the top platform had to be 7075-T6 aluminium alloy with the material properties listed in Table 6.1. In addition, the platform had a thickness of 8 mm.

Table 6.1: Material properties of 7050-T6 aluminium alloy - Modified from (Systemés 2017).

Category	**Type**	**E-modulus** [MPa]	**Poisons's ratio** [Nan]	**Density** [Kg/m^3]	**Yield strength** [MPa]	**Tensile strength** [MPa]
Aluminium alloys	7075-T6	72000	0.33	2810	505	570

It should be noted that the simulation conducted in SolidWorks is an idealised representation of the structure, where no cracks or ripples are present. This means that the Von Mises stresses and displacements found in the simulation are often underestimated. Therefore, a factor of safety (FOS) is often introduced to ensure that the structure was able to withstand the loads in reality. For the present simulations, it was a requirement to maintain a FOS of 1.5 or higher to ensure that the top platform would be able to withstand the loads present during an AP test.

The FOS is defined as the ratio between the yield strength and the maximum von Mises stress. The FOS is

given by:

$$\mathsf{FOS} = \frac{\sigma_Y}{\sigma_{VM}} \tag{6.1}$$

where 'σ_Y' is the yield strength of the material and 'σ_{VM}' is the maximum Von Mises stress during a load situation (Systemés 2017).

6.1.1 Boundary conditions

The top platform is fixed in the holes for the force transducer. A force of 271.91 N was applied in the holes, where the actuators are mounted to the top platform, to represent the maximum forces acting in an exaggerated situation where all actuators induce an equal amount of force (Figure 6.1).

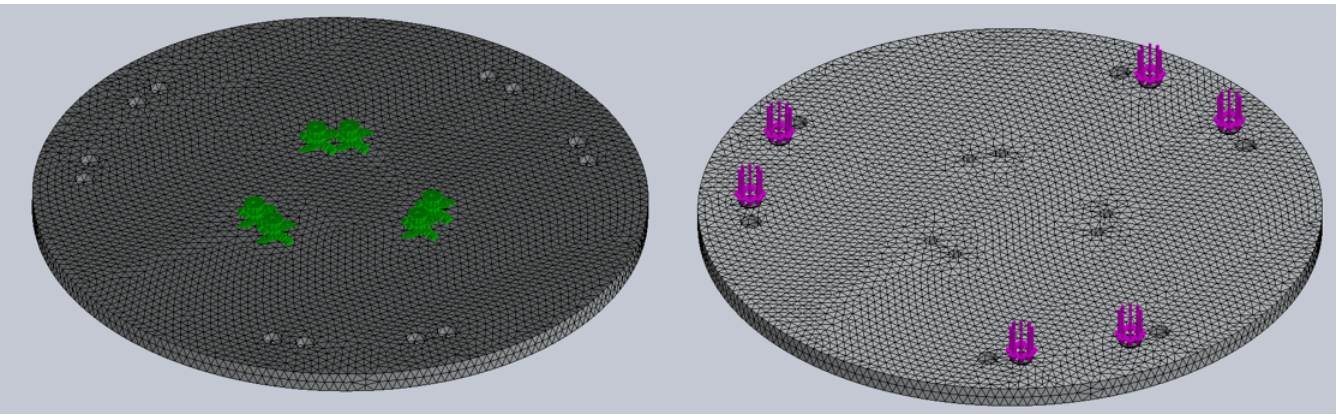

Figure 6.1: An illustration of the meshed top platform and boundary conditions. Left: Top view with the fixation points. Right: Bottom view with the applied forces.

6.1.1.1 Mesh

The number of elements and nodes along with the aspect ratio (AR) during the simulation can be seen in Table 6.2, and an example of the meshed top platform can be seen shown in figure 6.1. The platform was meshed using a solid mesh of high quality.

Table 6.2: Mesh details including number of elements, nodes, and aspect ratio (AR) details.

Number of Elements	Number of nodes	Maximum AR	Percentage with AR below 3
64202	101947	17.17	99.2

6.2 Results

The results from the simulations are listed in Table 6.3. In addition, a plot of the Von Mises stress throughout the top platform can be seen in Figure 6.2, a plot of the FOS throughout the top platform can be seen in Figure 6.3, and a plot of the displacement throughout the top platform can be seen in Figure 6.4.

Table 6.3: Results from SolidWorks finite element analysis simulation.

Max von Mises stress [MPa]	Min FOS [NaN]	Max displacement [mm]
51.32	9.84	0.18

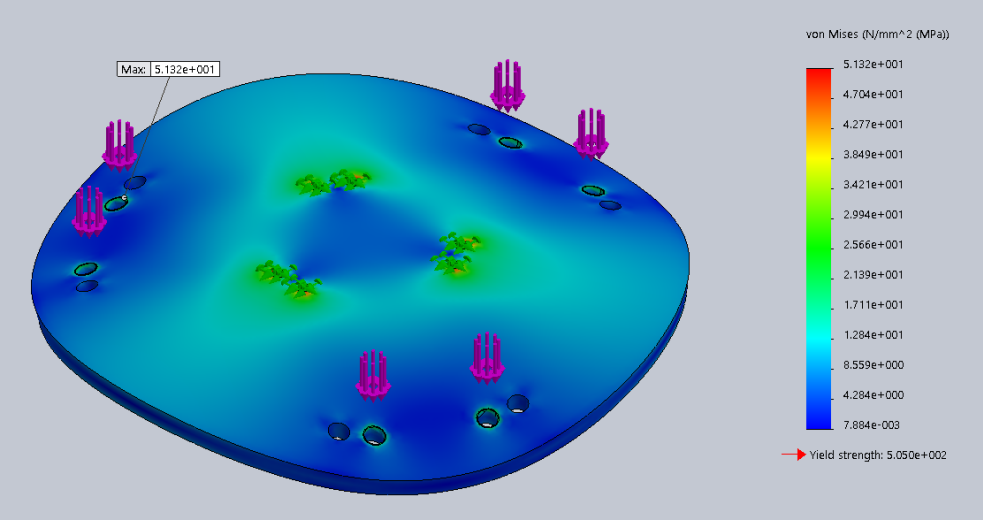

Figure 6.2: The von Mises stress throughout the top platform.

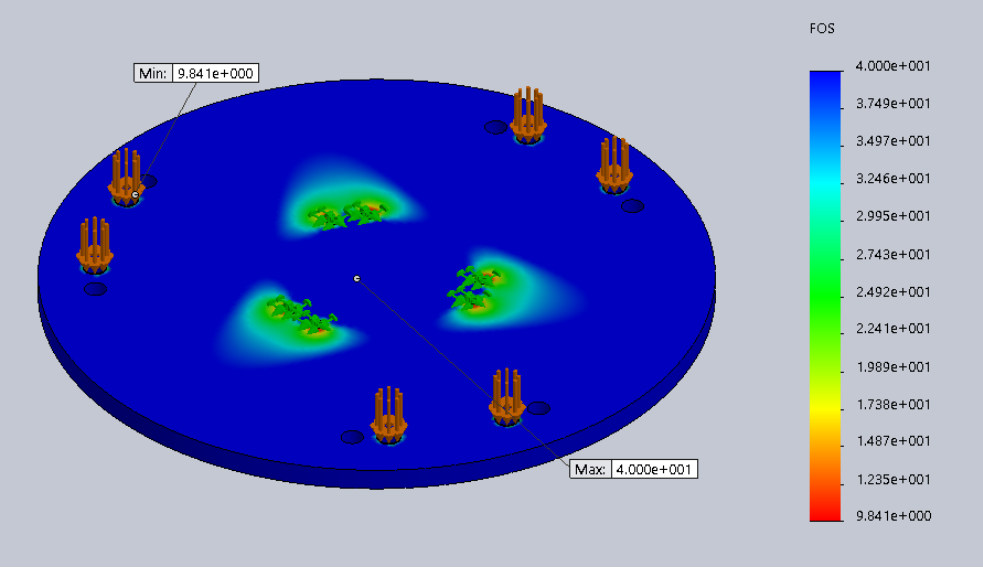

Figure 6.3: The factor of safety throughout the top platform.

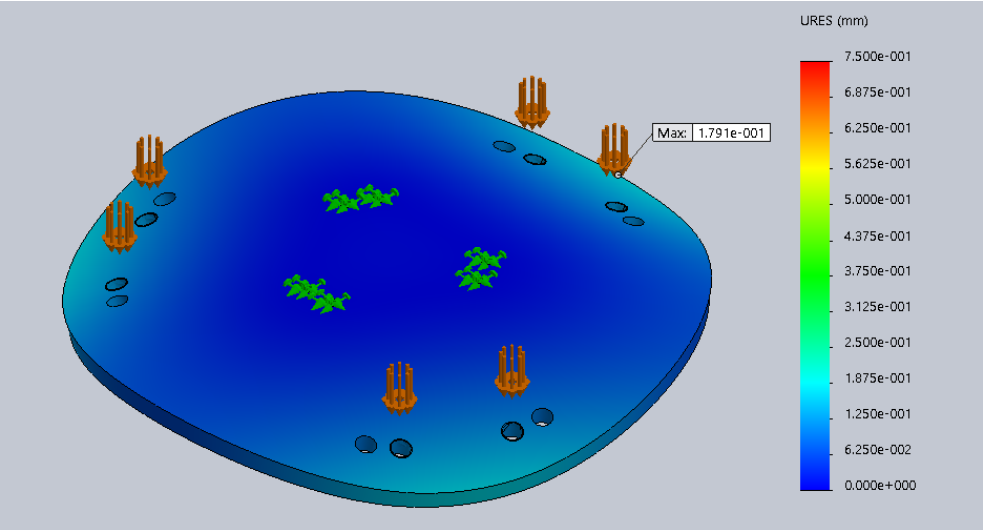

Figure 6.4: The displacement throughout the top platform.

The maximum Von Mises stress does not exceed the yield strength of the top platform. Thus, a top platform with a thickness of 8 mm made of 7075-T6 aluminium alloy can withstand the loads present during an exaggerated examination of knee laxity in accordance with the current literature.

6.2.1 Final configuration

The final configuration of the top and bottom platform would have a radius of 100 mm and 125 mm, respectively. Both platforms were made of 7075-T6 aluminium alloy and had a thickness of 8 mm. Technical drawings of the top and bottom platform can be seen in appendix A.1.2 and A.1.3, respectively.

Verification of range of motion 7

The following chapter includes a description of the test for verification of ROM, and the methods used for this. Furthermore, the results of the AP, VV, and IE ROM are presented individually.

To assess whether the arthrometer was capable of performing the necessary movements to stress the ligaments according to the current literature, a ROM verification test was conducted using motion capture. The purpose of the test was to demonstrate the mobility of the arthrometer during AP, VV, and IE static knee joint laxity examinations (Section 5.1).

7.1 Test setup

The test setup consisted of eight infrared cameras (Oqus 300 series, Qualisys, Gothenburg, Sweden) mounted around the arthrometer, to obtain motion capture data from all angles and prevent marker drop-out. Data was collected for two seconds in a static position with a sampling frequency of 100 Hz. Prior to recording data, a calibration of the cameras was conducted.

A total of five passive markers were attached to the arthrometer: one at the top (1) and bottom (5) platform centre, and three on the top platform, between coupled linear actuator pairs (2, 3, and 4) (Figure 7.1). Each marker was fixed with double-sided adhesive tape. Furthermore, the arthrometer was attached to the floor to avoid unnecessary movements, thereby minimising external factors.

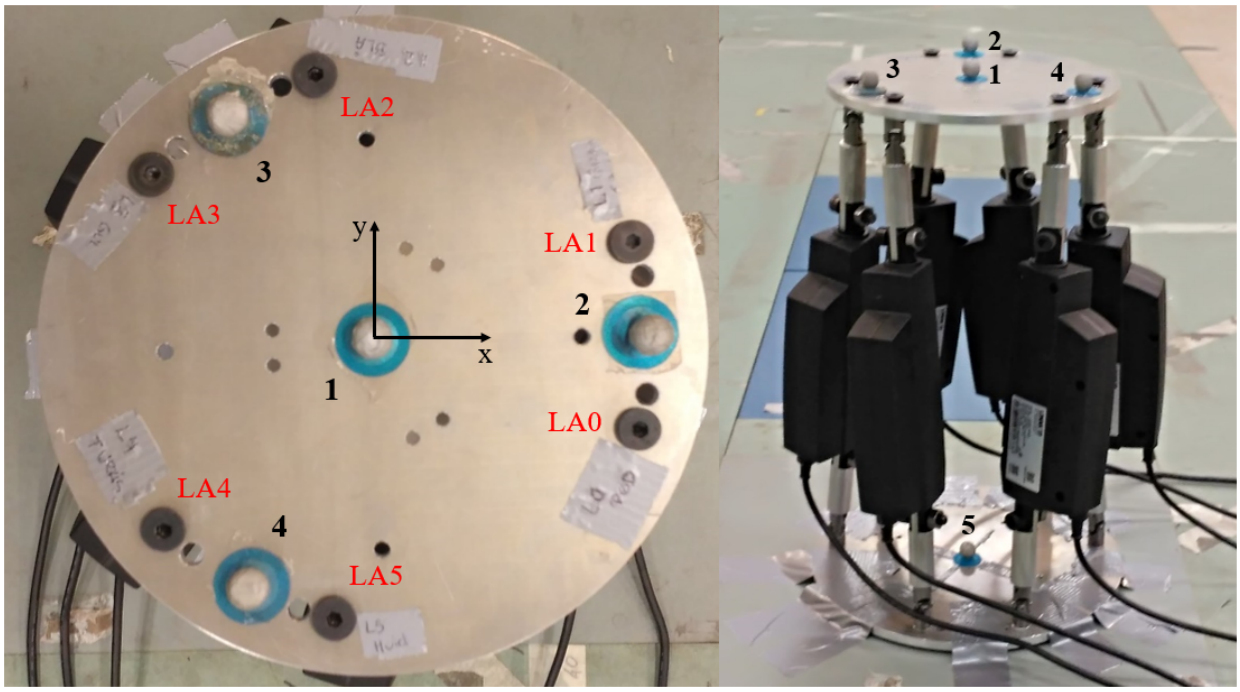

Figure 7.1: Left: The position of Marker 1, 2, 3, and 4 and linear actuators (LA0, LA1, LA2, LA3, LA4, and LA5) during the ROM verification test. Right: Position of Marker 1, 2, 3, 4, and 5 on the top and bottom platform.

7.2 Test protocol

For each test two static trials were conducted: a pre-trial and a post-trial. For the pre-trial, the actuators were positioned in fully retracted positions, thus, ensuring a consistent reference position of the top platform. For the post-trial, the top platform was positioned to resemble the AP, VV, and IE laxity examinations, by manual operation of the actuators by turns. Data were collected for six trials in pairs of three, each pair consisting of a pre-trial and a post-trial. Hence, an AP, VV, and IE ROM verification test were conducted.

7.2.1 Anterior-Posterior range of motion

For the AP test, LA3 and LA4 were fully extended to reproduce a situation of maximal AP translation. LA0, LA1, LA2, and LA5 were extended subsequently to obtain a horizontal level of the top platform (Figure 7.2).

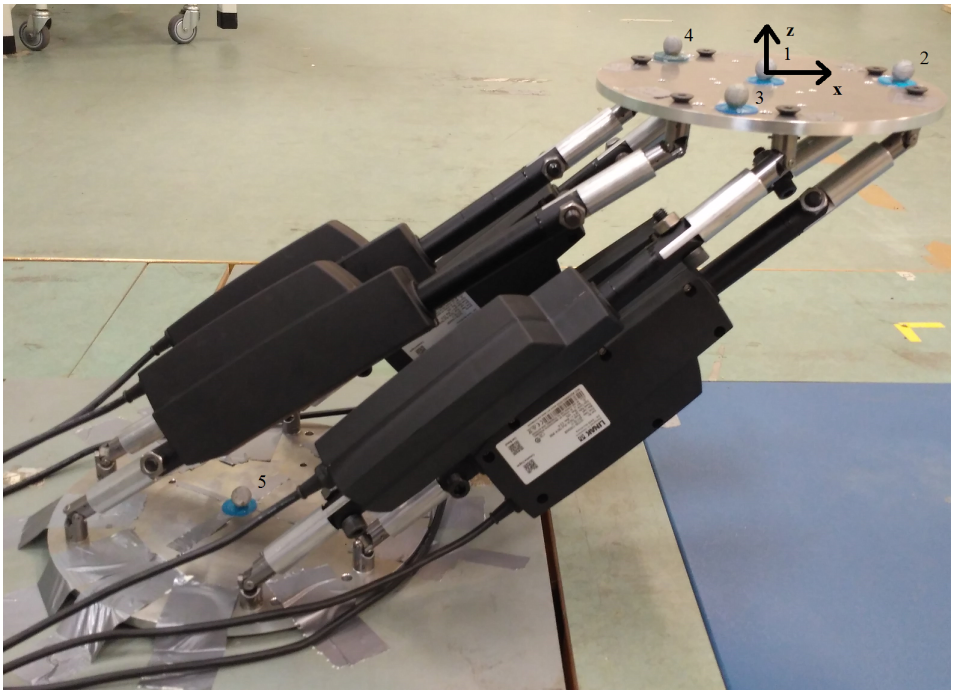

Figure 7.2: End position of the top platform during anterior-posterior laxity test.

7.2.2 Varus-valgus range of motion

For the VV test, each actuator extension was determined according to the VV simulation result, computed in AMS, due to the complexity of the movement (Table 7.1, Figure 7.3).

Table 7.1: The length of each actuator, based on the AnyBody Modelling System simulation performed with a varus-valgus rotation of 16.45°.

Actuator [nr.]	**Length** [mm]
LA0	492.42
LA1	475.52
LA2	502.91
LA3	509.93
LA4	456.71
LA5	466.72

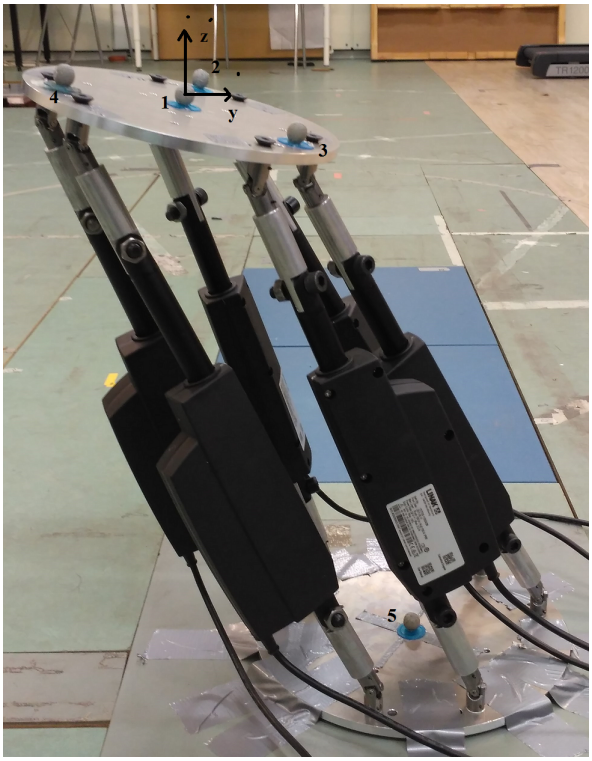

Figure 7.3: End position of the top platform during varus-valgus laxity test.

7.2.3 Internal-external range of motion

For the IE test, LA1, LA3, and LA5 were extended 20 mm to reproduce a situation of maximal IE rotation (Figure 7.4). It should be noted that the actuators are capable of extending more. However, this might result in a collapse of the arthrometer.

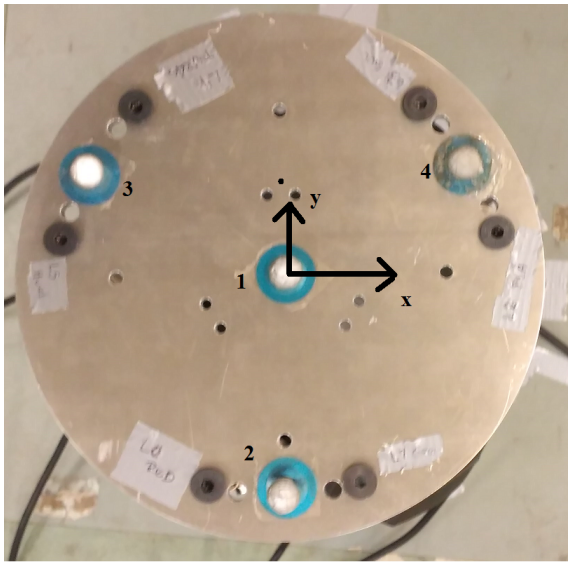

Figure 7.4: End position of the top platform during internal-external laxity test.

7.3 Data processing

The data were processed using Matlab (Mathworks, Inc; Natick, Massachusetts, USA).

7.3.1 Anterior-posterior

Marker 1 was used to calculate the translational displacement of the AP test (Figure 7.5). Equation (7.1) shows how the displacement was calculated.

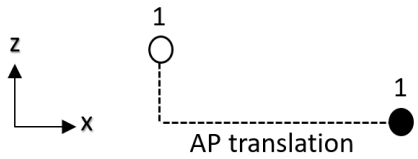

Figure 7.5: 2D illustration of the markers used for calculation of anterior-posterior range of motion. ◯: represent the markers in the pre trial. •: represent the markers in the post-trial.

$$AP_{translation} = 1_{post}(x) - 1_{pre}(x) \tag{7.1}$$

7.3.2 Varus-valgus

The VV rotation was calculated by creating a virtual marker representing the knee joint with a knee height of 550 mm perpendicular to the top platform (Figure 7.6). The VV rotation was calculated as shown in equation (7.2). Furthermore, as the top platform needs to be perpendicular to the tibia, the orientation of the top platform around the x-axis was also calculated (equation (7.3)). The markers were labelled in correspondence to Figure 7.3.

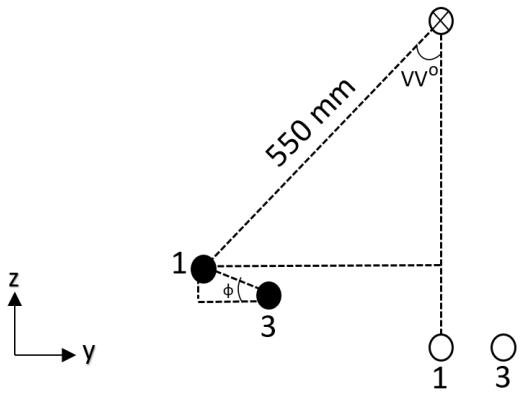

Figure 7.6: 2D illustration of the markers used for calculation of varus-valgus angular displacement. ◯: represent the markers in the pre trial. •: represent the markers in the post-trial. ⊗: represent the virtual marker.

$$VV^\circ = \sin^{-1}\left(\frac{1_{post}(y) - 1_{pre}(y)}{550}\right) \tag{7.2}$$

$$\Phi = \tan^{-1}\left(\frac{1_{post}(z) - 3_{post}(z)}{1_{post}(y) - 3_{post}(y)}\right) \tag{7.3}$$

7.3.3 Internal-External

The IE rotational displacement was calculated as illustrated in equation (7.4). A 2D illustration of the markers used in the calculation are shown in Figure 7.7. Vector $\vec{a}$ and $\vec{b}$, were created as shown in equation (7.4). The translational displacement was taken into account by calculating a mean (X) from the post and pre-trial of marker 1.

$$IE^\circ = \cos^{-1}\left(\frac{\vec{a}\cdot\vec{b}}{|\vec{a}|\cdot|\vec{b}|}\right) \tag{7.4}$$

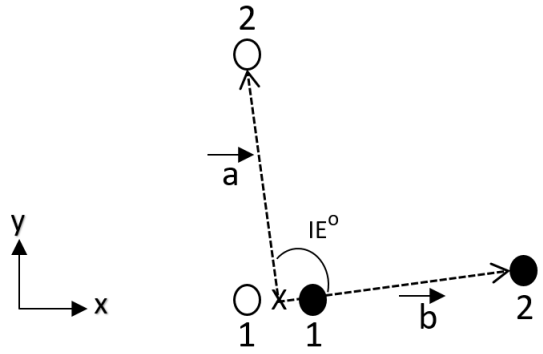

Figure 7.7: 2D illustration of the markers used for calculation of internal-external angular displacement. ◯: represents the markers in the pre trial. •: represent the markers in the post-trial and the X represents the mean of pre- and post-trial of marker 1

$$\vec{a} = \begin{pmatrix} 2_{pre}(x) - X(x) \\ 2_{pre}(y) - X(y) \end{pmatrix}, \vec{b} = \begin{pmatrix} 2_{post}(x) - X(x) \\ 2_{post}(y) - X(y) \end{pmatrix} \tag{7.5}$$

7.3.4 Displacement of the top platform

As the linear actuators were operated manually, the displacement of marker 1 in the x, y and z-direction was calculated to obtain the displacement directions of each test as this might limit the validity of the ROM

verification. Equation (7.6), (7.7) and (7.8) show the calculation of marker 1 displacement for each test.

$$\mathrm{Disp}_x = 1_{\mathrm{post}}(x) - 1_{\mathrm{pre}}(x) \tag{7.6}$$

$$\mathrm{Disp}_y = 1_{\mathrm{post}}(y) - 1_{\mathrm{pre}}(y) \tag{7.7}$$

$$\mathrm{Disp}_z = 1_{\mathrm{post}}(z) - 1_{\mathrm{pre}}(z) \tag{7.8}$$

7.4 Results

The results of the AP, VV and IE ROM verification tests are shown in Table 7.1, 7.2, and 7.3, respectively.

Table 7.2: Results from the anterior-posterior range of motion verification test.

$\mathbf{Disp}_x$ [mm]	$\mathbf{Disp}_y$ [mm]	$\mathbf{Disp}_z$ [mm]
383.41	20.67	-118.23

Table 7.3: Results from the varus-valgus range of motion verification test.

$\mathbf{VV}_{\mathrm{rot}}$ [deg]	ϕ [deg]	$\mathbf{Disp}_x$ [mm]	$\mathbf{Disp}_y$ [mm]	$\mathbf{Disp}_z$ [mm]
18.97	13.87	-47.52	178.78	32.13

Table 7.4: Results from the internal-external range of motion verification test.

$\mathbf{IE}_{\mathrm{rot}}$ [deg]	$\mathbf{Disp}_x$ [mm]	$\mathbf{Disp}_y$ [mm]	$\mathbf{Disp}_z$ [mm]
90.17	-6.02	0.21	-17.10

8 Discussion

The aim of the current thesis was to develop an arthrometer, based on the principles of a six DOF parallel manipulator, to assist objective examination of static knee joint laxity by stressing the ligaments according to the AP, VV and IE laxity examinations. The ROM verification test showed an AP translational displacement of 383.41 mm, VV angular displacement of 18.97° and an IE angular displacement of 90.17° (Section 7.4). Thus, the test indicates that the arthrometer is capable of performing the required movements according to the AP, VV, and IE static knee joint laxity examinations. However, these tests alone are not sufficient to determine the compatibility of the arthrometer for examination of laxity, due to simplified preliminary results.

8.1 Verification of range of motion

8.1.1 Anterior-posterior

The results from the AP ROM verification test showed that the arthrometer is capable of translating the top platform 383.41 mm in the x-direction (Section 7.2). According to the current AP laxity examination methods, the tibia is supposed to move translationally in one direction exclusively (Section 5.2). However, the y and z-translation of the top platform showed 20.67 mm and -118.23 mm, respectively.

The maximum AP laxity translation would be affected by these deviations. The deviation in the z-axis would decrease the translation, while the deviation in the y-axis would increase the translation. However, the effect of the y deviation would be less than the z deviation, leading to a maximum AP laxity translation smaller than the AP ROM. To avoid deviation in the z-axis, extension of the actuators is required to maintain the same vertical level of the top platform throughout the movement. In spite of these deviations, the difference between the AP ROM and the maximum AP translation from the current literature (17.2 mm) is 366.21 mm (Section 5.5.2). Thus, the arthrometer is most likely capable of performing the required movements for an AP laxity examination.

8.1.2 Varus-valgus

The results from the VV ROM verification test showed an angular displacement of 18.97° for the VV rotation (Section 7.4). The angular displacement of the VV rotation was 2.57° larger compared to the highest value in the current literature, 16.45°. (Section 5.5.2). However, as the top platform needs to be perpendicular to the tibia, the rotation of the top platform around the x-axis, ϕ, must be the same as the VV rotation. The results showed a top platform rotation of 13.87°, which does not correspond to the VV rotation of 18.97°. The difference of 5.10° might be explained by the limited control of the top platform, as each actuator were manually operated by turns. A small correction of any actuator would probably produce the required ϕ. Since the test was performed using the actuator lengths from the AMS simulations, the test did not assess the maximum VV rotation (7.1). When considering the rotation of the top platform and the angular displacement of the VV rotation, it is likely that the arthrometer is capable of performing the required movement for a VV laxity examination.

8.1.3 Internal-external

The results from the IE ROM verification test showed an angular displacement of 90.17° for the IE rotation (Section 7.4). Compared to the highest value in the current literature, the IE rotation of the arthrometer is 68.67° larger (Section 5.5.2). This indicate that the arthrometer is capable of performing the movement needed to examine static IE knee joint laxity.

According to the current methods regarding IE laxity examinations, the tibia is supposed to rotate around the vertical axis, z, exclusively (Section 5.2). However, the results for the translational displacement of the top platform in the x, y, and z-axes showed -6.02 mm, 0.21 mm and -17.10 mm, respectively. This indicate that the actual IE rotation might be smaller than reported. However, the actuators are capable of extending more than 20 mm, thereby, possibly increasing IE rotation. Despite these considerations, the arthrometer is most likely capable of performing the required movement for an IE laxity examination.

8.2 Arthrometer development

The conceptual idea presented in the thesis theoretically resolves most of the current problems regarding the examination of static knee joint laxity. As the focus of this thesis was the development of the arthrometer, the conceptual idea was not tested. This includes an evaluation of the interplay between the actuators and the force sensor as well as the practical application of the arthrometer within the EOS X-ray scanner. This

evaluation is necessary to describe the functionality of the concept in a real-life application. However, the conceptual idea is similar to the method presented by Pedersen et al. (2017) who determined static knee joint laxity in 3D from a cadaveric knee joint with regards to AP translation, IE rotation and mediolateral translation. The conceptual idea differs from the method of Pedersen et al. (2017) by enabling examination of VV rotation. Thus, the arthrometer presented in this thesis is also developed to assist in examinations of VV laxity, which is a frequent measurement of static knee joint laxity (Bignozzi et al. 2010, Shultz et al. 2012).

The required ROM of the arthrometer is based on the highest static knee joint laxity value from the current literature (Section 5.1). In spite of this, the possibility of individuals exceeding these laxity values cannot be disregarded. To account for this, a buffer of 25 % was implemented in the ROM and load capacity calculations (Section 5.1). However, because none of the configurations was applicable, the buffer was removed, thereby increasing the possibility of an insufficient ROM. Despite this, the results of the ROM verification test showed that the arthrometer exceeded the highest values in the current literature (Section 7.4). This indicate that individuals with higher laxity values compared to the current literature can also be examined by the arthrometer although the buffer was removed.

The size of the LA12 actuator housing resulted in a relocation of the holes on the platform from 12.5° to 20° to lower the risk of collision. This mean that the two joints in a joint pair were separated by 40° instead of the initial 25°. As this issue was realised after the actuators were received, simulations investigating if this would affect the ROM of the arthrometer were not performed. However, despite the relocation of the joints, the verification of ROM results indicate that the arthrometer has the required ROM to obtain the highest laxity values from the current literature.

8.3 Finite element analysis

The results of the FEA showed that an 8 mm top platform manufactured in 7075-T6 aluminium alloy has a maximum von Mises stress of 51.32 MPa when simulating an exaggerated load scenario (Section 6.2). As 7075-T6 aluminium alloy has a yield strength of 505 MPa, the results indicate that the top platform would be capable of withstanding the forces induced through AP, VV, and IE laxity examinations.

The minimum FOS was 9.84, which indicate a design optimisation might be appropriate (Section 6.3). The material and thickness were based on the accessibility and durability of the 7075-T6 aluminium alloy, without evaluations regarding the cost of production. However, as the FOS was larger than the permitted FOS of 1.5, a subsequent simulation regarding design iteration, could have been conducted to estimate potential

cost or manufacturing optimisations.

Apart from limitations occurring when conducting FEA, other confounding factors might have influenced the simulation results (Section 3.2.2). A fine mesh quality was used for discretization of the top platform for the FEA (Section 6.1.1.1). Even though a higher mesh quality entails a more precise estimation of a model, it increases the computational demands of the FEA (Dassault-Systemés 2017). As the geometrical structure of the top platform is relatively simple, it was deemed important to enhance the mesh quality to attain a better estimation of the physical behaviour.

A force of 271.91 N was used for the FEA (Section 6.1.1). The load was applied perpendicular to the holes of the top platform, by creating a surrounding circular extrusion (Section 6.1). Furthermore, the fixation points were an approximation of the actual location. In reality, the load is more likely split between the intermediate components, connecting the actuators to the aircast boot. Hence, several components risk yielding, and not just the top platform. A subsequent FEA, including all of the components, might be requisite to estimate the actual physical behaviour of the arthrometer.

The force was applied in the holes to simulate an exaggerated load scenario. However, compared to the AMS simulations, this does not replicate the actual forces present during the examination of static knee joint laxity, as the force is not equal in the holes. In spite of this, a minimum FOS of 9.84 indicates that the top platform was capable of withstanding the applied forces, even in the exaggerated load scenario (Section 6.3).

9 Conclusion

This thesis presents an arthrometer based on the principles of a six DOF parallel manipulator. It is developed to assist objective examination of static knee joint laxity by stressing the ligaments according to the AP, VV, and IE laxity examinations. The results of the ROM verification test showed an AP translational displacement of 383.41 mm, a VV angular displacement of 18.97° and an IE angular displacement of 90.17°. These results exceed the highest values reported in the current literature. Thus, the arthrometer presented has the potential to assist objective examinations of static AP, VV, and IE knee joint laxity.

Even though the size of the arthrometer is determined in relation to the dimensions of an EOS X-ray scanner, future studies should evaluate the practical application of the arthrometer in conjunction with the EOS X-ray scanner. Position control is requisite for this purpose. Furthermore, the arthrometer should be validated through comparison to the currently available methods, which quantifies static knee joint laxity.

Bibliography

Abdellatif, H. & Heimann, B. (2009), 'Computational efficient inverse dynamics of 6-dof fully parallel manipulators by using the lagrangian formalism', *Mechanism and Machine Theory* **44**(1), 192–207.

Adler, G. G., Hoekman, R. A. & Beach, D. M. (1995), 'Drop leg lachman test', *The American Journal of Sports Medicine* **23**(3), 320–323.

Andersen, M. S., Damsgaard, M. & Rasmussen, J. (2009), 'Kinematic analysis of over-determinate biomechanical systems', *Computer Methods in Biomechanics and Biomedical Engineering* **12**(4), 371–384.

AnyBody-Technology (2017*a*), 'Anybody tutorials - inverse dynamics', Internet. http://www.anybodytech.com/fileadmin/AnyBody/Docs/Tutorials/chap4_A_study_of_studies/lesson4.html.

AnyBody-Technology (2017*b*), 'Anybody tutorials - kinematic analysis', Internet. http://www.anybodytech.com/fileadmin/AnyBody/Docs/Tutorials/Making-things-move/lesson3.html.

AnyBody-Technology (2017*c*), 'Anybody tutorials - parameter studies', Internet. http://www.anybodytech.com/fileadmin/AnyBody/Docs/Tutorials/chap12_Parameter_studies_and_optimization/intro.html.

Balonov, M. I. & Shrimpton, P. C. (2012), 'Effective dose and risks from medical x-ray procedures', *Annals of the ICRP* **41**(1), 129 – 141.

Becerra-Vargas, M. & Morgado Belo, E. (2012), 'Application of h∞ theory to a 6 dof flight simulator motion base', *Journal of the Brazilian Society of Mechanical Sciences and Engineering* **34**(2), 193–204.

Bignozzi, S., Zaffagnini, S., Lopomo, N., Fu, F. H., Irrgang, J. J. & Marcacci, M. (2010), 'Clinical relevance of static and dynamic tests after anatomical double-bundle acl reconstruction', *Knee Surg Sports Traumatol Arthrosc* **18**(1), 37–42.

Bingul, Z. & Karahan, O. (2012), *Dynamic modeling and simulation of stewart platform*, INTECH Open Access Publisher.

Branch, T. P., Mayr, H. O., Browne, J. E., Campbell, J. C., Stoehr, A. & Jacobs, C. A. (2010), 'Instrumented examination of anterior cruciate ligament injuries: minimizing flaws of the manual clinical examination', *Arthroscopy: The Journal of Arthroscopic & Related Surgery* **26**(7), 997–1004.

Charters, T., Enguiça, R. & Freitas, P. (2009), 'Detecting singularities of stewart platforms', *Mathematics-in-Industry Case Studies Journal* **1**, 66–80.

Colombet, P., Robinson, J., Christel, P., Franceschi, J.-P. & Djian, P. (2007), 'Using navigation to measure rotation kinematics during acl reconstruction.', *Clinical orthopaedics and related research* **454**, 59–65.

Craig, J. (2005), *Introduction to Robotics: Mechanics and Control*, third edn, Prentice Hall.

Creaby, M. W., Wrigley, T. V., Lim, B. W., Bowles, K.-A., Metcalf, B. R., Hinman, R. S. & Bennell, K. L. (2010), 'Varus-valgus laxity and passive stiffness in medial knee osteoarthritis', *Arthritis care & research* **62**(9), 1237–1243.

Damsgaard, M., Rasmussen, J., Christensen, S. T., Surma, E. & De Zee, M. (2006), 'Analysis of musculoskeletal systems in the anybody modeling system', *Simulation Modelling Practice and Theory* **14**(8), 1100 – 1111.

Dasgupta, B. & Mruthyunjaya, T. (1998), 'A newton-euler formulation for the inverse dynamics of the stewart platform manipulator', *Mechanism and machine theory* **33**(8), 1135–1152.

Dasgupta, B. & Mruthyunjaya, T. (2000), 'The stewart platform manipulator: a review', *Mechanism and machine theory* **35**(1), 15–40.

Dassault-Systemés (2017), *SolidWorks Educational Edition*, Dassault Systemés, Waltham, Massachusetts, USA. http://help.solidworks.com/2016/English/SolidWorks/install_guide/HID_STATE_MANUAL_DOWNLOAD.htm.

Freisinger, G. M., Hutter, E. E., Lewis, J., Granger, J. F., Glassman, A. H., Beal, M. D., Pan, X., Schmitt, L. C., Siston, R. A. & Chaudhari, A. M. W. (2016), 'Relationships between varus-valgus laxity of the severly osteoarthritic knee and gait, instability, clinical performance, and function', *Journal of Orthopeadic research* pp. 1–9.

Ganko, A., Engebresten, L. & Ozer, H. (2000), 'The rolimeter. a new arthrometer compared with the kt-1000', *Knee Surgery, Sports Traumatology, Arthroscopy* **8**(1), 36–39.

Garavaglia, G., Lubbeke, A., Dubois-Ferriere, V., Suva, D., Fritschy, D. & Menetrey, J. (2007), 'Accuracy of stress radiography techniques in grading isolated and combined posterior knee injuries a cadaveric study', *The American journal of sports medicine* **35**(12), 2051–2056.

Ghobakhloo, A., Eghtesad, M. & Azadi, M. (2006), Position control of a stewart-gough platform using inverse dynamics method with full dynamics, *in* 'Advanced Motion Control, 2006. 9th IEEE International Workshop on', IEEE, pp. 50–55.

Harrison, C. R. & Robinette, K. M. (2002), Caesar: Summary statistics for the adult population (ages 18-65) of the united states of america, Technical report, DTIC Document.

Hoshino, Y., Araujo, P., Ahlden, M., Moore, C. G., Kuroda, R., Zaffaginini, S., Karlsson, J., Fu, F. H. & Musahl, V. (2012), 'Standardized pivot shift test improves measurement accuracy', *Knee Surgery, Sports Traumatology, Arthroscopy* **20**(1), 732–736.

Illés, T. & Somoskeöy, S. (2012), 'The eos™ imaging system and its uses in daily orthopaedic practice', *International orthopaedics* **36**(7), 1325–1331.

Jean-Yves, J., Puliero, B., Schockmel, G., Harnoist, S. & Clavert, P. (2017), 'Experimental validation of the gnrb for measuring anterior tibial translation', *Orthopaedics and Traumatology: Surgery and Research* .

Kakarlapudi, T. K. (2001), 'Knee instability: isolated and complex', *British Journal of Sports Med.* **34**(1), 394–400.

Komdeur, P., Pollo, F. E. & Jackson, R. W. (2002), 'Dynamic knee motion in anterior cruciate impairment: a report and case study', *Proceedings (Baylor University. Medical Center)* **15**(3), 257.

Küpper, J., Loitz-Ramage, B., Corr, D., Hart, D. & Ronsky, J. (2007), 'Measuring knee joint laxity: a review of applicable models and the need for new approaches to minimize variability', *Clinical Biomechanics* **22**(1), 1–13.

Küçük, S. (2012), *Serial and Parallel Robot Manipulators – Kinematics, Dynamics, Control and Optimization,*, first edition edn, InTech.

Linak (2017), 'Linak danmark a/s', Internet. https://www.linak.com/.

Lopes, A. M. (2009), 'Dynamic modeling of a stewart platform using the generalized momentum approach', *Communications in Nonlinear Science and Numerical Simulation* **14**(8), 3389–3401.

Markolf, K. L., Park, S., Jackson, S. R. & McAllister, D. R. (2008), 'Simulated pivot-shift testing with single and double-bundle anterior cruciate ligament reconstructions', *The Journal of Bone & Joint Surgery* **90**(8), 1681–1689.

Martelli, S., Lopomo, N., Bignozzi, S., Zaffagnini, S. & Visani, A. (2007), 'Validation of a new protocol for navigated intraoperative assessment of knee kinematics', *Computers in biology and medicine* **37**(6), 872–878.

Martini, F. H., Nath, J. L. & Bartholomew, E. F. (2012), *Fundamentals of Anatomy & Physiology*, ninth edition edn, Pearson Education Inc.

Miyazaki, T., Uchida, K., Wada, M., Sato, M., Sugita, D., Shimada, S. & Baba, H. (2012), 'Anteroposterior and varus–valgus laxity of the knee increase after stair climbing in patients with mild osteoarthritis', *Rheumatology international* **32**(9), 2823–2828.

Moewis, P., Boeth, H., Heller, M. O., Yntema, C., Jung, T., Doyscher, R., Ehrig, R. M., Zhong, Y. & Taylor, W. R. (2014), 'Towards understanding knee joint laxity: Errors in non-invasive assessment of joint rotation can be corrected', *Medican Engineering & Physics* **36**(1), 889–895.

Mouton, C., Theisen, D., Pape, D., Nührenbörger, C. & Seil, R. (2012), 'Static rotational knee laxity in anterior cruciate ligament injuries', *Knee Surgery, Sports Traumatology, Arthroscopy* **20**(4), 652–662.

Mueller, J. & Rosenfeld, S. (2017), 'Electric linear actuators with feedback sensors', Internet. http://www.timotion.com/white_paper/Part%207-Feedback%20Sensors%20of%20an%20Actuator_20161107.pdf.

Mura, A. (2011), 'Six dof displacement measuring device based on a modified stewart platform', *Mechatronics* **21**(8), 1309–1316.

Musahl, V., Karlsson, J., Kuroda, R. & Zaffagnini, S. (2017), *Rotatory Knee Instability*, Springer.

Nair, R. & Maddocks, J. H. (1994), 'On the forward kinematics of parallel manipulators', *The International Journal of Robotics Research* **13**(2), 171–188.

Nanua, P., Waldron, K. J. & Murthy, V. (1990), 'Direct kinematic solution of a stewart platform', *IEEE Transactions on Robotics and Automation* **6**(4), 438–444.

Narasaiah, G. L. (2008), *Narasaiah, G. L.*, ed. 5.5 edn, BS Publications.

Pedersen, D., Vanheule, V., Wirix-Speetjens, R., Taylan, O., Delport, H. P., Scheys, L. & Skipper, M. (2017), Knee joint laxity in 3d.

Robertson, C. & Hamill, K. W. (2004), *Research Methods in Biomechanics*, first edition edn, Human Kinetics.

RS-Components (2017), 'Rs components a/s', Internet. http://dk.rs-online.com/web/p/kardanled/7906693/.

Schipani, P. & Marty, L. (2006), Stewart platform kinematics and secondary mirror aberration control, *in* 'SPIE Astronomical Telescopes+ Instrumentation', International Society for Optics and Photonics, pp. 62733B–62733B.

Schmitt, L. C., Fitzgerald, G. K., Reisman, A. S. & Rudolph, K. S. (2008), 'Instability, laxity, and physical function in patients with medial knee osteoarthritis', *Physical therapy* **88**(12), 1506.

Schmitz, R. J., Ficklin, T. K., Shimokochi, Y., Nguyen, A.-D., Beynnon, B. D., Perrin, D. H. & Shultz, S. J. (2008), 'Varus/valgus and internal/external torsional knee joint stiffness differs between sexes', *The American journal of sports medicine* **36**(7), 1380–1388.

Scholten, R. P. M., Opstelten, W., v. d. Plaas, C., Biji, D., Deville, W. L. J. M. & Bouter, L. M. (2003), 'Accuracy of physical diagnostic test for assessing ruptures of the anterior crutiate ligament: A meta-analysis', *The Journal of Family Practice* **52**(9), 689–694.

Sharma, L., Lou, C., Felson, D. T., Dunlop, D. D., Kirwan-Mellis, G., Hayes, K. W., Weinrach, D. & Buchanan, T. S. (1999), 'Laxity in healthy and osteoarthritic knees', *Arthritis & Rheumatism* **42**(5), 861–870.

Shultz, M. S., Russe, K., Lampakis, G. & Strobel, M. J. (2005), 'Reliability of stress radiography for evaluation of posterior knee laxity', *The American Journal of Sports Medicine* **33**(4), 502 – 506.

Shultz, S. J., Pye, M. L., Montgomery, M. M. & Schmitz, R. J. (2012), 'Associations between lower extremity muscle mass and multiplanar knee laxity and stiffness', *The American Journal of Sports Medicine* **40**(12), 2836–2844.

Shultz, S. J., Shimokochi, Y., Nguyen, A.-D., Schmitz, R. J., Beynnon, B. D. & Perrin, D. H. (2007), 'Measurement of varus-valgus and internal–external rotational knee laxities in vivo—part i: assessment of measurement reliability and bilateral asymmetry', *Journal of orthopaedic research* **25**(8), 981–988.

Snyder-Mackler, L., Fitzgerald, G. K., Bartolozzi, A. R. & Ciccotti, M. G. (1997), 'The relationship between passive joint laxity and functional outcome after anterior cruciate ligament injury', *The American Journal of Sports Medicine* **25**(2), 191–195.

Song, E. K., Seon, J. K., Park, S. J., Hur, C. I. & Lee, D. S. (2009), 'In vivo laxity of stable versus anterior cruciate liagment-injured knees using a navigation system: a comparative study', *Knee Surgery, Sports Traumatology, Arthroscopy* **17**(8), 941–945.

Stewart, D. (1965), 'A platform with six degrees of freedom', *Proceedings of the institution of mechanical engineers* **180**(1), 371–386.

Su, Y., Duan, B., Peng, B. & Nan, R. (2003), 'Singularity analysis of fine-tuning stewart platform for large radio telescope using genetic algorithm', *Mechatronics* **13**(5), 413–425.

Sundemo, D., Alentorn-Geli, E., Hoshino, Y., Musahl, V., Karlsson, J. & Samuelsson, K. (2016), 'Objective measures on knee instability. dynamic test. a review of devices for assessment of dynamic knee laxity through utilization of the pivot shift test', *Curr Rev Musculoskelet Med* **9**(1), 148–159.

Systemés, D. (2017), 'Solidworks educational edition', Internet.
URL: *https://www.solidworks.com/*

Taylor, J. B., Wang, H.-M., Schmitz, R. J., Rhea, C. K., Ross, S. E. & Shultz, S. J. (2015), 'Multiplanar knee laxity and perceived function during activities of daily living and sport', *Journal of athletic training* **50**(11), 1199–1206.

Thomas, A. C., Hubbard-Turner, T., Wikstrom, E. A. & Palmieri-Smith, R. M. (2016), 'Epidemiology of posttraumatic osteoarthritis', *Journal of athletic training* .

Torii, A., Banno, M., Ueda, A. & Doki, K. (2012), 'A small-size self-propelled stewart platform', *Electrical Engineering in Japan* **2**(181), 37–46.

Ulrich, K. T. & Eppinger, S. D. (2004), *Product Design and Development*, first edition edn, McGraw-Hill/Irwin.

Van Eck, C. F., van den Bekerom, M. P., Fu, F. H., Poolman, R. W. & Kerkhoffs, G. M. (2013), 'Methods to diagnose acute anterior cruciate ligament rupture: a meta-analysis of physical examinations with and without anaesthesia', *Knee Surgery, Sports Traumatology, Arthroscopy* **21**(8), 1895–1903.

Wybier, M. & Bossard, P. (2013), 'Musculoskeletal imaging in progress: the eos imaging system', *Joint Bone Spine* **80**(3), 238–243.

Yamamoto, Y., Ishibashi, Y., Tsuda, E., Tsukada, H., Maeda, S. & Toh, S. (2010), 'Comparison between clinical grading and navigation data of knee laxity in acl-deficient knees', *BMC Sports Science, Medicine and Rehabilitation* **2**(1), 27.

Zantop, T., Herbort, M., Raschke, M. J., Fu, F. H. & Petersen, W. (2007), 'The role of the anteromedial and posterolateral bundles of the anterior cruciate ligament in anterior tibial translation and internal rotation', *The American journal of sports medicine* **35**(2), 223–227.

Zar, J. H. (2010), *Biostatistical Analysis*, fifth edition edn, Pearson, Upper Saddle River, New Jersey 07458.

Appendix A

A.1 Technical Drawings

A.1.1 LA12

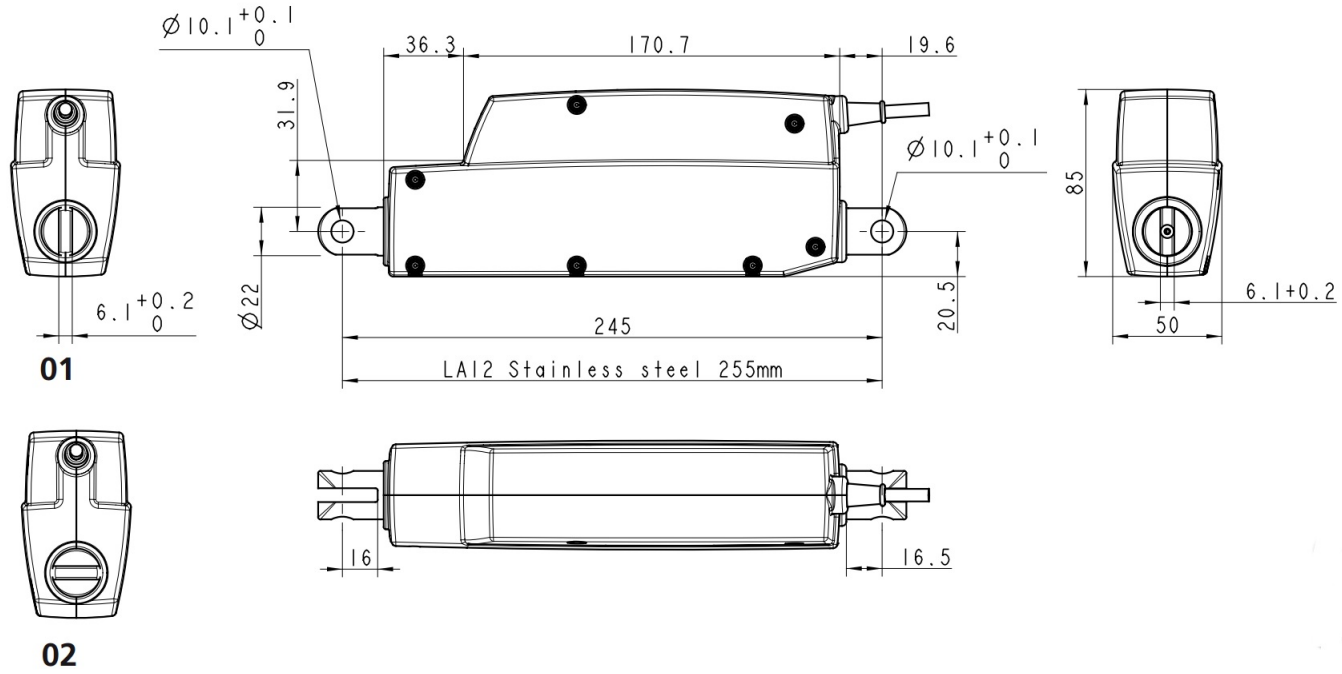

Figure A.1: The technical drawing of the LA12 (Linak 2017)

A.1.2 Top Platform

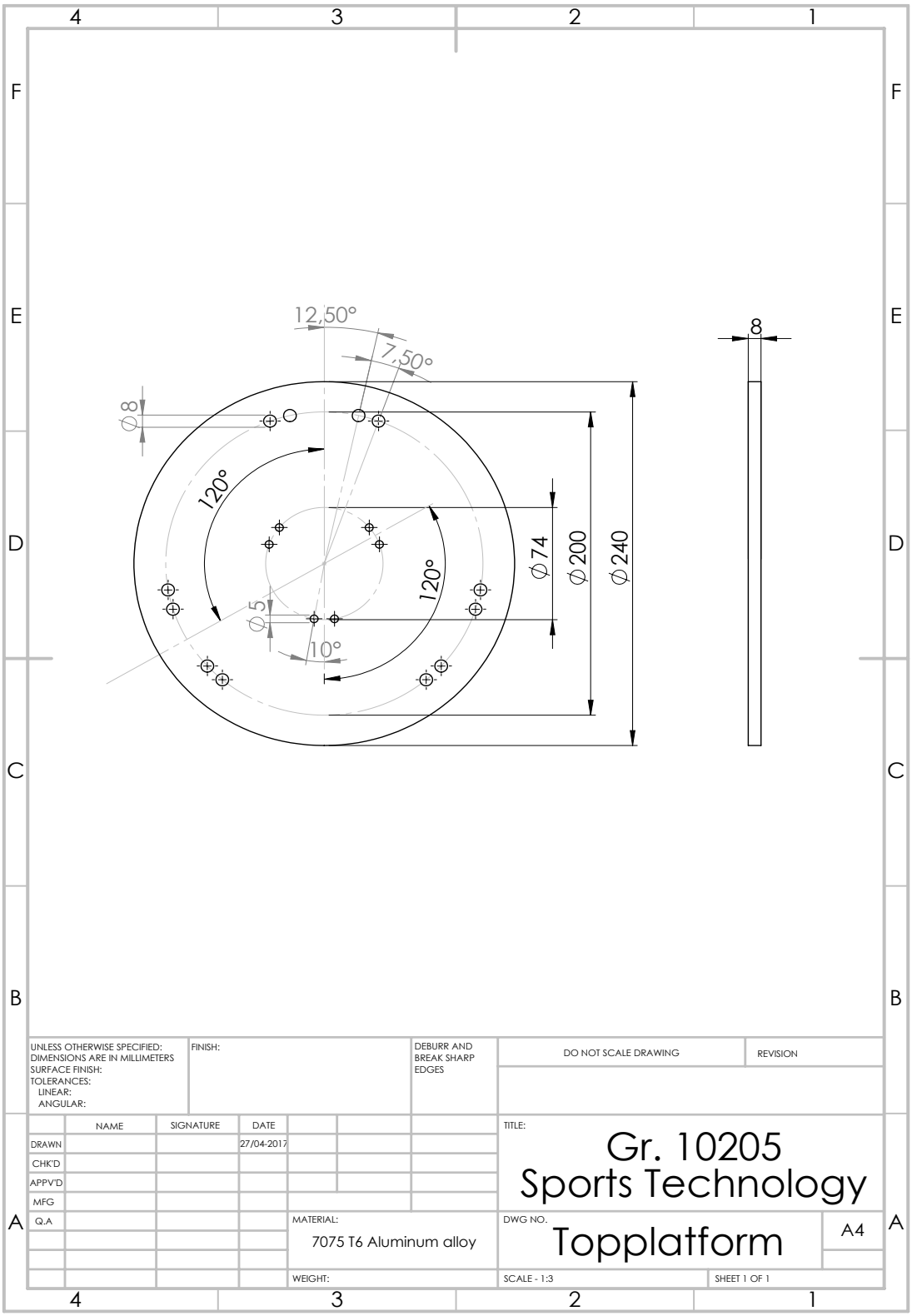

Figure A.2: The technical drawing of the top platform. The dimensions given are in mm and degrees.

A.1.3 Bottom platform

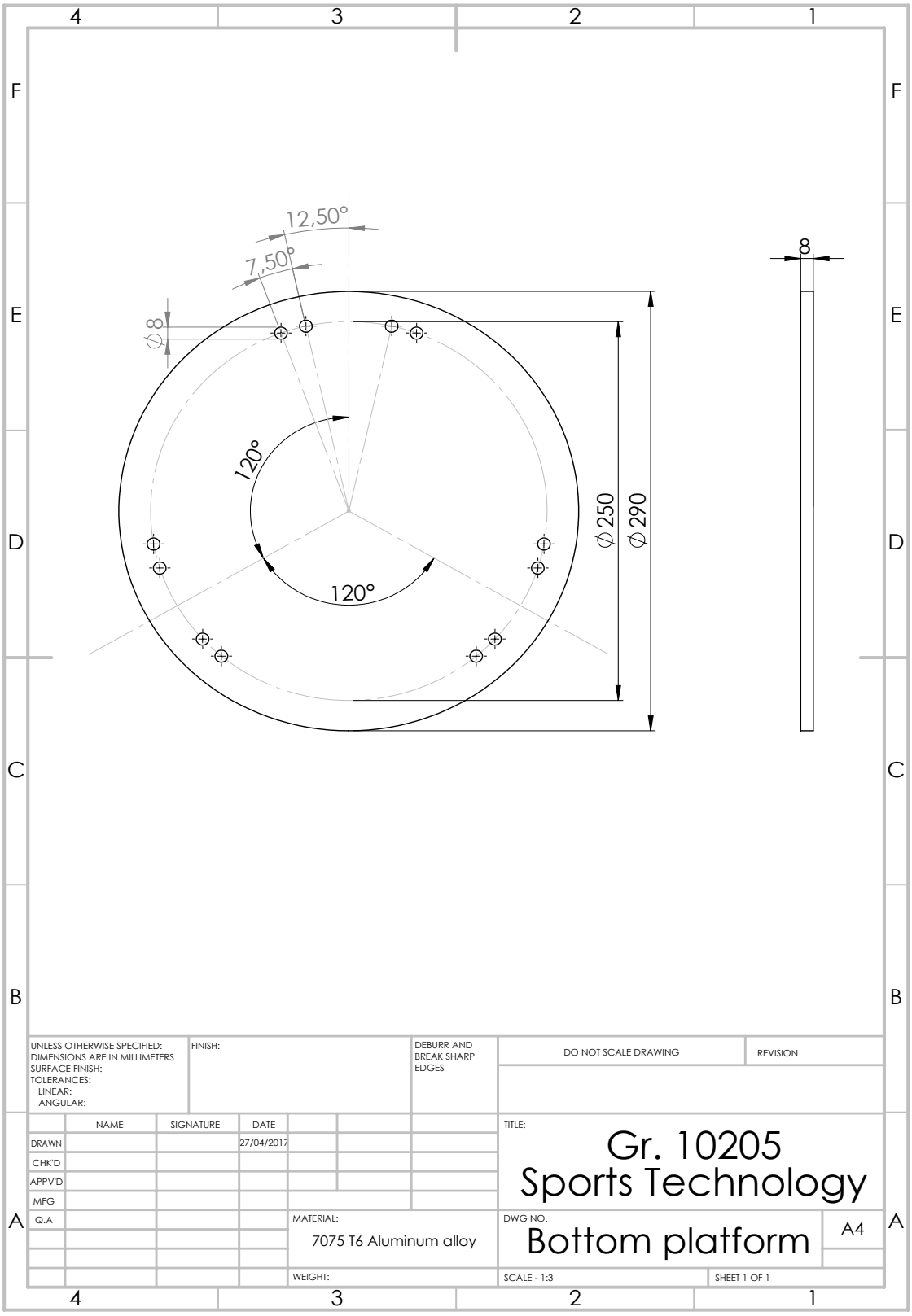

Figure A.3: The technical drawing of the bottom platform. The dimensions given are in mm and degrees.

A.1.4 Linking part

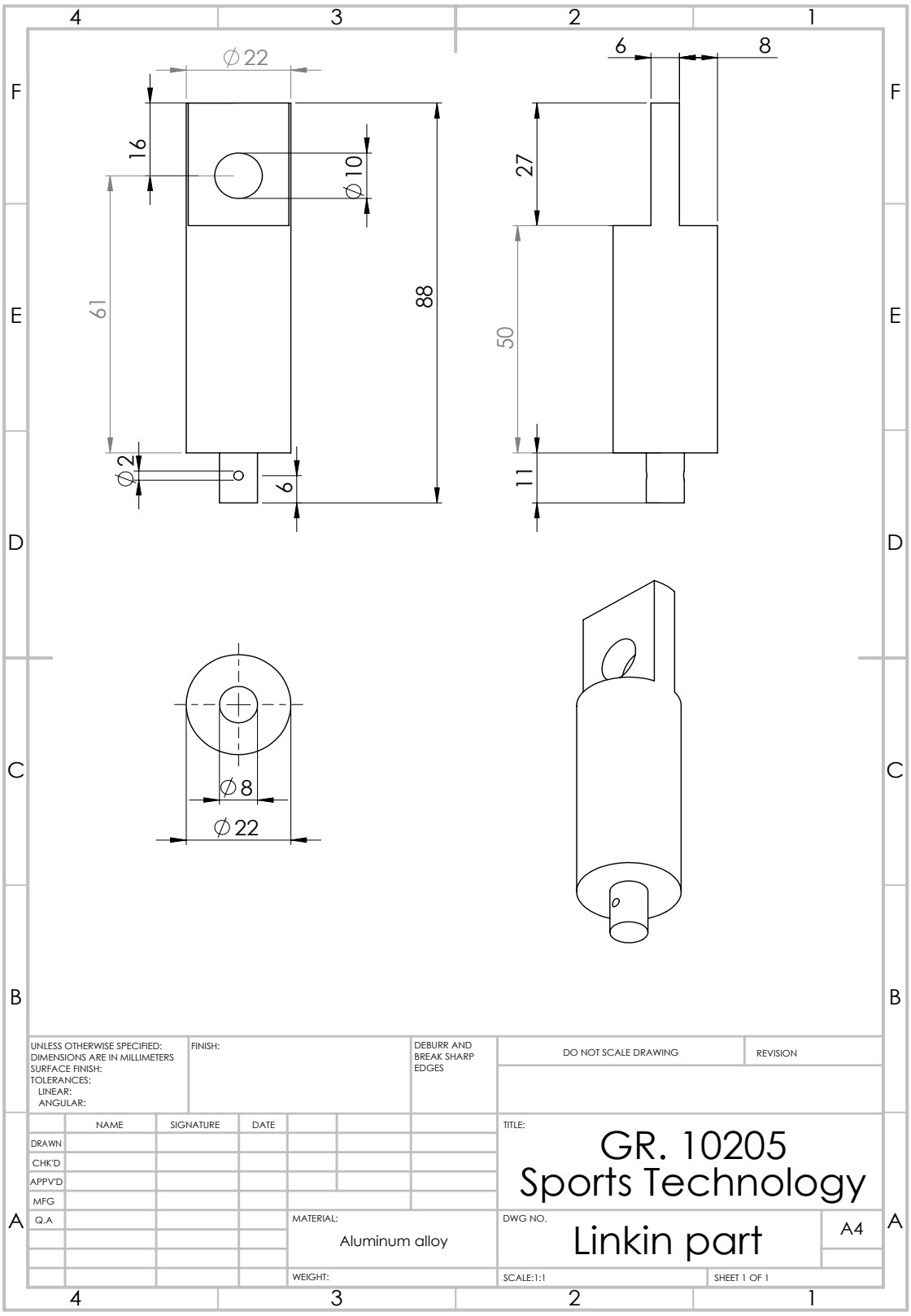

Figure A.4: The technical drawing of the linking part. The dimensions given are in mm and degrees.

A.1.5 RS Pro universal joint

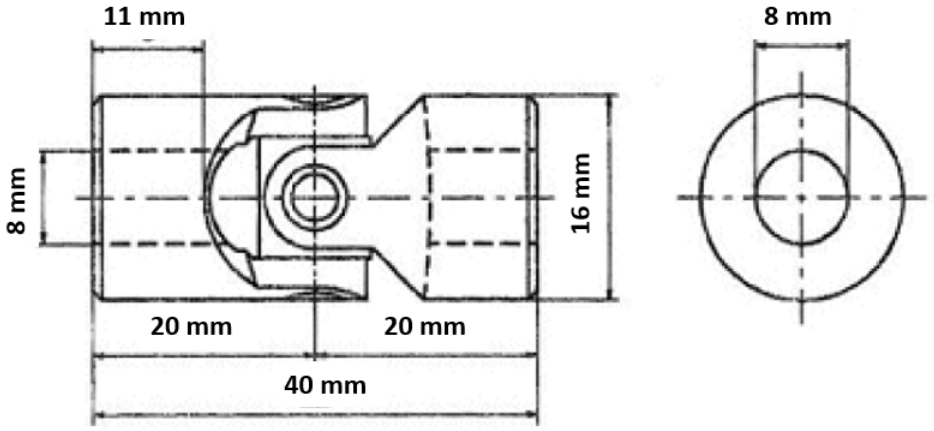

Figure A.5: The technical drawing of the RS Pro universal joints. The dimensions given are in mm. - Modified from RS-Components (2017).

A.2 Components

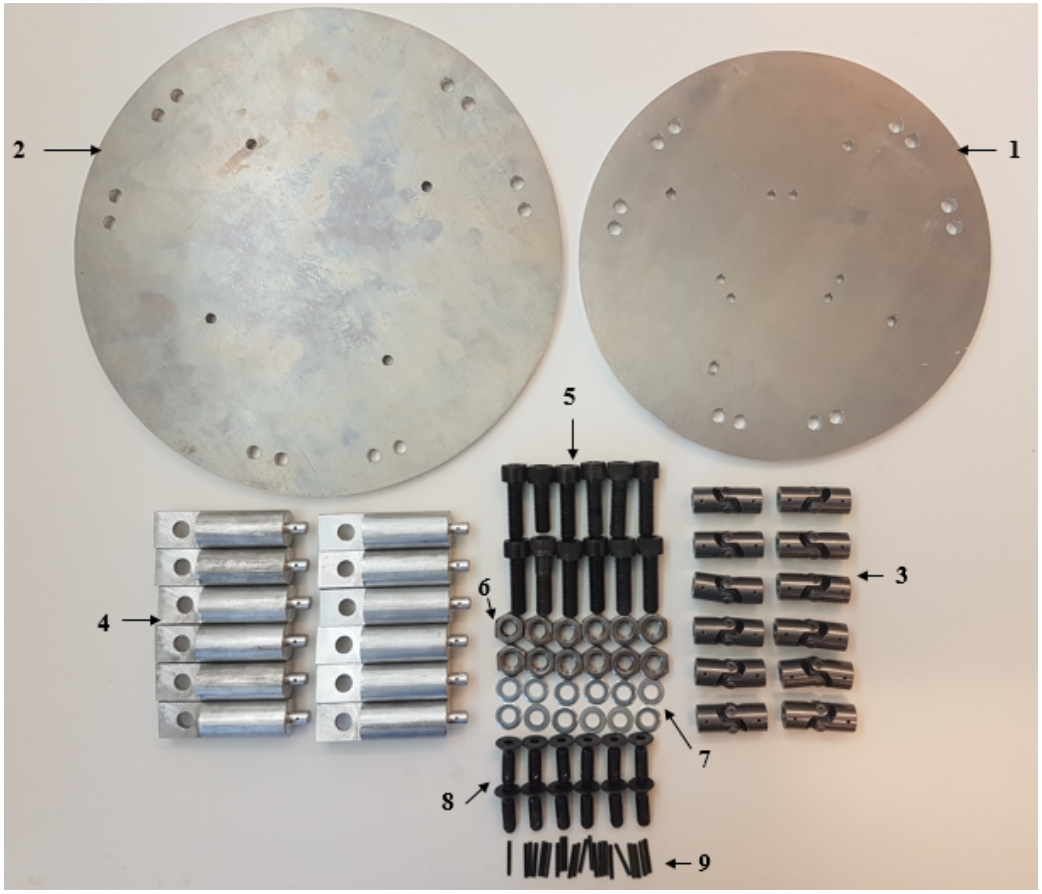

Figure A.6: An overview of all the components (excluding the linear actuators) used for the final assembly of the arthrometer. This includes the top platform (1), the bottom platform (2), 12 universal joints (3), 12 linking parts (4), 12 M10x35 mm bolts (5), 12 Ø10 mm nuts (6), 12 washers (7), 12 M8x25 mm bolts (8), and 24 pins (9).

Figure A.7: Six La12IC linear actuators and appurtenant power supplies.

A.3 AnyBody simulations

Table A.1: The AnyBody Modelling System simulation results from the varus-valgus test around the x-axis and the maximum force from the anterior-posterior test in the x-axis.

Nr.	Top platform [mm]	Bottom platform [mm]	Height [mm]	LA_{min} [mm]	LA_{max} [mm]	Stroke length [mm]	BID [mm]	LA_{max}/LA_{min} [NaN]	Max Force [N]
1	100	100	100	63,24	277,12	213,88	-150,64	4,38	92,30
2	100	100	150	109,79	302,46	192,67	-82,88	2,75	136,30
3	100	100	200	158,45	333,43	174,98	-16,52	2,10	185,46
4	100	100	250	207,74	368,60	160,86	46,88	1,77	236,18
5	100	100	300	257,30	406,89	149,59	107,71	1,58	287,59
6	100	100	350	306,99	447,49	140,50	166,49	1,46	339,33
7	100	100	400	356,77	489,84	133,07	223,71	1,37	391,29
8	100	100	450	406,60	533,51	126,91	279,70	1,31	443,36
9	100	100	500	456,47	578,21	121,74	334,73	1,27	495,55
10	100	125	100	67,59	285,87	218,28	-150,69	4,23	81,59
11	100	125	150	116,55	305,08	188,53	-71,98	2,62	113,32
12	100	125	200	165,01	332,56	167,55	-2,54	2,02	150,90
13	100	125	250	212,81	367,81	155,00	57,81	1,73	190,47
14	100	125	300	261,43	406,18	144,74	116,69	1,55	230,95
15	100	125	350	310,49	446,85	136,36	174,13	1,44	271,91
16	100	125	400	359,79	489,25	129,45	230,34	1,36	313,15
17	100	125	450	409,27	532,97	123,70	285,57	1,30	354,57
18	100	125	500	458,85	577,71	118,85	340,00	1,26	396,10
19	100	150	100	69,32	303,17	233,85	-164,53	4,37	77,79
20	100	150	150	118,59	321,35	202,76	-84,18	2,71	100,91
21	100	150	200	167,96	345,85	177,89	-9,93	2,06	130,18
22	100	150	250	217,42	375,46	158,03	59,39	1,73	161,89
23	100	150	300	266,95	409,05	142,09	124,86	1,53	194,77
24	100	150	350	315,86	447,59	131,73	184,13	1,42	228,31
25	100	150	400	364,46	489,93	125,47	238,99	1,34	262,23
26	100	150	450	413,39	533,60	120,21	293,18	1,29	296,40
27	100	150	500	462,54	578,29	115,75	346,79	1,25	330,75
28	100	175	100	75,53	321,48	245,95	-170,42	4,26	76,33
29	100	175	150	123,45	338,68	215,22	-91,77	2,74	93,81
30	100	175	200	172,14	362,01	189,87	-17,73	2,10	117,02
31	100	175	250	221,15	390,39	169,24	51,91	1,77	142,89
32	100	175	300	270,35	422,80	152,45	117,90	1,56	170,17
33	100	175	350	319,66	458,38	138,71	180,95	1,43	198,24
34	100	175	400	369,07	496,45	127,38	241,70	1,35	226,81
35	100	175	450	418,55	536,48	117,93	300,62	1,28	255,71
36	100	175	500	467,50	579,94	112,44	355,06	1,24	284,84
37	100	200	100	85,30	340,65	255,35	-170,05	3,99	75,48
38	100	200	150	130,88	356,92	226,04	-95,16	2,73	89,45
39	100	200	200	178,32	379,13	200,82	-22,50	2,13	108,26
40	100	200	250	226,53	406,32	179,79	46,74	1,79	129,70

Table A.2: Continued table from previous page

Nr.	Top platform [mm]	Bottom platform [mm]	Height [mm]	LA_{min} [mm]	LA_{max} [mm]	Stroke length [mm]	BID [mm]	LA_{max}/LA_{min} [NaN]	Max Force [N]
41	100	200	300	275,15	437,55	162,39	112,76	1,59	152,67
42	100	200	350	324,03	472,01	147,98	176,05	1,46	176,55
43	100	200	400	373,10	509,07	135,97	237,12	1,36	201,03
44	100	200	450	422,29	548,18	125,89	296,40	1,30	225,90
45	100	200	500	471,58	588,94	117,36	354,22	1,25	251,05
46	125	100	100	54,59	294,12	239,53	-184,95	5,39	97,32
47	125	100	150	103,78	319,13	215,35	-111,56	3,07	140,03
48	125	100	200	153,49	349,54	196,05	-42,56	2,28	188,99
49	125	100	250	203,33	384,08	180,75	22,57	1,89	239,64
50	125	100	300	253,23	421,73	168,50	84,72	1,67	291,00
51	125	100	350	303,15	461,73	158,58	144,57	1,52	342,72
52	125	100	400	353,10	503,52	150,42	202,68	1,43	394,65
53	125	100	450	403,05	546,69	143,63	259,42	1,36	446,72
54	125	100	500	453,02	590,93	137,92	315,10	1,30	498,87
55	125	125	100	65,12	291,40	226,28	-161,16	4,47	79,46
56	125	125	150	109,77	316,63	206,85	-97,08	2,88	112,54
57	125	125	200	157,65	347,26	189,61	-31,96	2,20	150,91
58	125	125	250	206,52	382,00	175,49	31,03	1,85	190,97
59	125	125	300	255,82	419,84	164,02	91,80	1,64	231,76
60	125	125	350	305,34	460,00	154,66	150,67	1,51	272,94
61	125	125	400	354,99	501,93	146,95	208,04	1,41	314,34
62	125	125	450	404,72	545,23	140,51	264,21	1,35	355,88
63	125	125	500	454,51	589,59	135,07	319,44	1,30	397,52
64	125	150	100	72,03	298,47	226,43	-154,40	4,14	72,99
65	125	150	150	120,09	316,61	196,52	-76,43	2,64	97,84
66	125	150	200	165,38	346,77	181,39	-16,00	2,10	128,36
67	125	150	250	212,52	381,56	169,04	43,48	1,80	160,90
68	125	150	300	260,71	419,43	158,72	101,99	1,61	194,34
69	125	150	350	309,47	459,63	150,16	159,32	1,49	228,27
70	125	150	400	358,56	501,59	143,03	215,54	1,40	262,50
71	125	150	450	407,88	544,92	137,04	270,84	1,34	296,90
72	125	150	500	457,33	589,30	131,97	325,37	1,29	331,43
73	125	175	100	72,54	315,45	242,91	-170,38	4,35	71,29
74	125	175	150	121,55	332,67	211,12	-89,57	2,74	89,82
75	125	175	200	170,72	356,14	185,42	-14,70	2,09	114,25
76	125	175	250	219,99	384,70	164,71	55,28	1,75	141,03
77	125	175	300	267,78	420,51	152,73	115,06	1,57	168,96
78	125	175	350	315,48	460,62	145,14	170,34	1,46	197,53
79	125	175	400	363,78	502,50	138,72	225,06	1,38	226,47
80	125	175	450	412,48	545,75	133,27	279,21	1,32	255,66
81	125	175	500	461,46	590,07	128,61	332,85	1,28	285,02
82	125	200	100	77,50	333,45	255,95	-178,45	4,30	71,32
83	125	200	150	125,85	349,78	223,94	-98,09	2,78	85,40
84	125	200	200	174,60	372,17	197,57	-22,98	2,13	105,12
85	125	200	250	223,56	399,59	176,03	47,52	1,79	127,40
86	125	200	300	272,67	431,09	158,42	114,25	1,58	151,02
87	125	200	350	321,89	465,83	143,94	177,96	1,45	175,42
88	125	200	400	370,56	504,64	134,08	236,48	1,36	200,29
89	125	200	450	418,49	547,72	129,23	289,26	1,31	225,48
90	125	200	500	466,85	591,89	125,04	341,80	1,27	250,89
91	150	100	100	49,88	312,20	262,32	-212,44	6,26	115,82
92	150	100	150	99,79	336,83	237,04	-137,25	3,38	152,09
93	150	100	200	149,74	366,65	216,91	-67,18	2,45	197,88
94	150	100	250	199,71	400,52	200,82	-1,11	2,01	246,77
95	150	100	300	249,68	437,49	187,81	61,87	1,75	297,04

Table A.3: Continued table from previous page

Nr.	Top platform [mm]	Bottom platform [mm]	Height [mm]	LA_{min} [mm]	LA_{max} [mm]	Stroke length [mm]	BID [mm]	LA_{max}/LA_{min} [NaN]	Max Force [N]
96	150	100	350	299,66	476,85	177,19	122,47	1,59	348,02
97	150	100	400	349,64	518,04	168,40	181,24	1,48	399,41
98	150	100	450	399,63	560,67	161,04	238,59	1,40	451,07
99	150	100	500	449,61	604,43	154,81	294,80	1,34	502,91
100	150	125	100	54,08	308,00	253,93	-199,85	5,70	83,58
101	150	125	150	102,04	332,94	230,90	-128,87	3,26	115,50
102	150	125	200	151,30	363,09	211,79	-60,50	2,40	153,40
103	150	125	250	200,91	397,26	196,35	4,56	1,98	193,30
104	150	125	300	250,67	434,51	183,84	66,83	1,73	234,08
105	150	125	350	300,50	474,11	173,61	126,89	1,58	275,25
106	150	125	400	350,38	515,52	165,14	185,23	1,47	316,65
107	150	125	450	400,28	558,34	158,06	242,22	1,39	358,19
108	150	125	500	450,20	602,27	152,07	298,14	1,34	399,83
109	150	150	100	67,49	305,80	238,31	-170,81	4,53	71,40
110	150	150	150	109,84	330,90	221,07	-111,23	3,01	97,10
111	150	150	200	156,72	361,22	204,49	-47,77	2,30	128,19
112	150	150	250	205,07	395,55	190,48	14,58	1,93	161,07
113	150	150	300	254,04	432,95	178,90	75,14	1,70	194,75
114	150	150	350	303,34	472,68	169,34	134,00	1,56	228,85
115	150	150	400	352,83	514,21	161,37	191,46	1,46	263,19
116	150	150	450	402,44	557,13	154,68	247,76	1,38	297,69
117	150	150	500	452,14	601,14	149,01	303,13	1,33	332,29
118	150	175	100	77,48	311,31	233,84	-156,36	4,02	67,12
119	150	175	150	122,14	330,75	208,61	-86,47	2,71	86,99
120	150	175	200	165,64	361,08	195,43	-29,79	2,18	112,41
121	150	175	250	212,01	395,42	183,41	28,60	1,87	139,87
122	150	175	300	259,71	432,83	173,12	86,59	1,67	168,25
123	150	175	350	308,13	472,57	164,44	143,69	1,53	197,14
124	150	175	400	356,98	514,11	157,13	199,84	1,44	226,33
125	150	175	450	406,10	557,04	150,94	255,16	1,37	255,71
126	150	175	500	455,40	601,06	145,65	309,75	1,32	285,23
127	150	200	100	76,94	328,00	251,05	-174,11	4,26	66,47
128	150	200	150	125,39	344,32	218,93	-93,53	2,75	81,56
129	150	200	200	174,19	366,78	192,59	-18,40	2,11	102,31
130	150	200	250	221,47	396,87	175,40	46,07	1,79	125,37
131	150	200	300	267,53	434,15	166,62	100,90	1,62	149,56
132	150	200	350	314,77	473,78	159,01	155,76	1,51	174,38
133	150	200	400	362,75	515,22	152,47	210,28	1,42	199,57
134	150	200	450	411,20	558,06	146,87	264,33	1,36	225,01
135	150	200	500	459,97	602,01	142,04	317,93	1,31	250,62
136	175	100	100	50,36	331,18	280,82	-230,46	6,58	140,54
137	175	100	150	98,11	355,40	257,29	-159,17	3,62	168,58
138	175	100	200	147,35	384,63	237,28	-89,93	2,61	210,12
139	175	100	250	196,96	417,81	220,85	-23,89	2,12	256,51
140	175	100	300	246,72	454,09	207,36	39,36	1,84	305,16
141	175	100	350	296,56	492,77	196,21	100,36	1,66	355,01
142	175	100	400	346,45	533,34	186,89	159,55	1,54	405,59
143	175	100	450	396,35	575,40	179,04	217,31	1,45	456,62
144	175	100	500	446,28	618,63	172,35	273,93	1,39	507,97
145	175	125	100	46,32	325,68	279,36	-233,04	7,03	97,24
146	175	125	150	96,19	350,28	254,09	-157,89	3,64	124,59
147	175	125	200	146,13	379,90	233,77	-87,64	2,60	160,37
148	175	125	250	196,09	413,46	217,37	-21,29	2,11	199,00
149	175	125	300	246,05	450,09	204,04	42,01	1,83	238,90
150	175	125	350	296,02	489,09	193,07	102,95	1,65	279,46

Table A.4: Continued table from previous page

Nr.	Top platform [mm]	Bottom platform [mm]	Height [mm]	LA_{min} [mm]	LA_{max} [mm]	Stroke length [mm]	BID [mm]	LA_{max}/LA_{min} [NaN]	Max Force [N]
151	175	125	400	345,99	529,94	183,95	162,05	1,53	320,42
152	175	125	450	395,97	572,25	176,27	219,70	1,45	361,62
153	175	125	500	445,95	615,71	169,75	276,20	1,38	403,00
154	175	150	100	54,32	322,03	267,71	-213,39	5,93	74,94
155	175	150	150	100,40	346,89	246,49	-146,09	3,46	99,60
156	175	150	200	149,00	376,78	227,78	-78,78	2,53	130,25
157	175	150	250	198,28	410,59	212,32	-14,04	2,07	162,89
158	175	150	300	247,83	447,46	199,63	48,20	1,81	196,42
159	175	150	350	297,52	486,67	189,15	108,37	1,64	230,52
160	175	150	400	347,30	527,71	180,41	166,89	1,52	264,87
161	175	150	450	397,12	570,18	173,06	224,07	1,44	299,38
162	175	150	500	446,98	613,78	166,80	280,19	1,37	333,99
163	175	175	100	70,37	320,30	249,92	-179,55	4,55	66,01
164	175	175	150	110,04	345,28	235,24	-125,21	3,14	86,39
165	175	175	200	155,72	375,29	219,57	-63,85	2,41	112,22
166	175	175	250	203,42	409,24	205,81	-2,39	2,01	139,92
167	175	175	300	252,00	446,21	194,21	57,80	1,77	168,49
168	175	175	350	301,03	485,52	184,49	116,54	1,61	197,50
169	175	175	400	350,33	526,65	176,32	174,00	1,50	226,78
170	175	175	450	399,79	569,20	169,41	230,38	1,42	256,24
171	175	175	500	449,37	612,87	163,51	285,86	1,36	285,81
172	175	200	100	83,78	324,39	240,62	-156,84	3,87	62,96
173	175	200	150	123,84	345,47	221,64	-97,80	2,79	79,06
174	175	200	200	165,84	375,47	209,63	-43,79	2,26	100,61
175	175	200	250	211,32	409,40	198,08	13,24	1,94	124,21
176	175	200	300	258,46	446,36	187,90	70,55	1,73	148,78
177	175	200	350	306,48	485,66	179,18	127,31	1,58	173,87
178	175	200	400	355,04	526,78	171,73	183,31	1,48	199,27
179	175	200	450	403,95	569,32	165,37	238,58	1,41	224,87
180	175	200	500	453,09	612,98	159,90	293,19	1,35	250,61
181	200	100	100	56,01	350,92	294,91	-238,91	6,27	168,71
182	200	100	150	98,96	374,73	275,77	-176,81	3,79	188,54
183	200	100	200	146,44	403,35	256,91	-110,47	2,75	225,35
184	200	100	250	195,17	435,85	240,68	-45,51	2,23	268,74
185	200	100	300	244,41	471,42	227,01	17,40	1,93	315,35
186	200	100	350	293,90	509,43	215,52	78,38	1,73	363,76
187	200	100	400	343,54	549,95	206,41	137,13	1,60	413,27
188	200	100	450	393,27	592,65	199,39	193,88	1,51	463,48
189	200	100	500	442,63	636,42	193,79	248,84	1,44	514,17
190	200	125	100	43,82	344,27	300,45	-256,63	7,86	116,55
191	200	125	150	92,71	368,50	275,80	-183,09	3,97	137,71
192	200	125	200	142,34	397,58	255,23	-112,89	2,79	170,19
193	200	125	250	192,15	430,51	238,36	-46,21	2,24	206,83
194	200	125	300	242,03	466,49	224,46	17,57	1,93	245,43
195	200	125	350	291,95	504,86	212,92	79,03	1,73	285,08
196	200	125	400	341,88	545,13	203,24	138,64	1,59	325,38
197	200	125	450	391,83	586,89	195,06	196,77	1,50	366,08
198	200	125	500	441,79	629,85	188,06	253,72	1,43	407,06
199	200	150	100	43,58	339,33	295,75	-252,17	7,79	85,46
200	200	150	150	92,71	363,89	271,18	-178,47	3,93	106,74
201	200	150	200	142,41	393,31	250,90	-108,49	2,76	135,77
202	200	150	250	192,25	426,57	234,33	-42,08	2,22	167,48
203	200	150	300	242,14	462,86	220,72	21,41	1,91	200,42
204	200	150	350	292,06	501,51	209,45	82,60	1,72	234,01
205	200	150	400	341,99	542,02	200,03	141,96	1,58	267,99

Table A.5: Continued table from previous page

Nr.	Top platform [mm]	Bottom platform [mm]	Height [mm]	LA_{min} [mm]	LA_{max} [mm]	Stroke length [mm]	BID [mm]	LA_{max}/LA_{min} [NaN]	Max Force [N]
206	200	150	450	391,94	584,00	192,06	199,88	1,49	302,21
207	200	150	500	441,89	627,16	185,27	256,62	1,42	336,60
208	200	175	100	55,43	336,18	280,75	-225,32	6,07	69,14
209	200	175	150	98,97	360,96	261,99	-163,02	3,65	88,59
210	200	175	200	146,64	390,60	243,96	-97,32	2,66	114,00
211	200	175	250	195,45	424,07	228,62	-33,17	2,17	141,47
212	200	175	300	244,72	460,56	215,83	28,89	1,88	169,89
213	200	175	350	294,23	499,39	205,16	89,07	1,70	198,80
214	200	175	400	343,87	540,06	196,19	147,68	1,57	228,05
215	200	175	450	393,59	582,18	188,59	205,01	1,48	257,52
216	200	175	500	443,38	625,47	182,09	261,29	1,41	287,10
217	200	200	100	73,78	334,88	261,10	-187,32	4,54	62,23
218	200	200	150	110,43	359,74	249,32	-138,89	3,26	78,62
219	200	200	200	154,69	389,47	234,79	-80,10	2,52	100,45
220	200	200	250	201,62	423,04	221,42	-19,81	2,10	124,24
221	200	200	300	249,71	459,61	209,89	39,82	1,84	148,93
222	200	200	350	298,42	498,51	200,09	98,34	1,67	174,12
223	200	200	400	347,49	539,24	191,76	155,73	1,55	199,59
224	200	200	450	396,78	581,43	184,65	212,13	1,47	225,24
225	200	200	500	446,22	624,77	178,55	267,67	1,40	251,02